



Geochemistry of coal mine drainage, groundwater, and brines from the Ibbenbüren mine, Germany: A coupled elemental-isotopic approach

Thomas Rinder^{a,*}, Martin Dietzel^b, Jessica A. Stammer^{b,c}, Albrecht Leis^d,
Diego Bedoya-González^{a,e}, Sylke Hilberg^a

^a University of Salzburg, Department of Geography and Geology, Hellbrunner Str. 34, 5020, Salzburg, Austria

^b Graz University of Technology, Institute of Applied Geosciences, Rechbauerstraße 12, 8010, Graz, Austria

^c GFZ German Research Centre for Geosciences, Telegrafenberg, 14473, Potsdam, Germany

^d JR-AquaConSol GmbH, Steyrergasse 21, 8010, Graz, Austria

^e University of Greifswald, Institute for Geography and Geology, Friedrich-Ludwig-Jahn Str. 17a, 17487, Greifswald, Germany

ARTICLE INFO

Editorial handling by Prof. M. Kersten

Keywords:

Coal mine drainage
Pyrite oxidation
Brine origin
Sulfur isotopic composition
Isotope proxies
Hydrogeochemistry

ABSTRACT

A coupled elemental-isotopic approach is applied to reconstruct the origin and chemical evolution of mine drainage, groundwater, and brines from the Carboniferous anthracite coal mine in Ibbenbüren, Germany. All solutions are characterized by an increase in salinity with depth, as well as by an increase in $^{34}\text{S}/^{32}\text{S}$ isotopic ratios of dissolved SO_4^{2-} . Br/Cl and Na/Cl ratios in deep Na-Cl-type water indicate halite dissolution as the common source of salinity. $\delta^{34}\text{S}_{\text{SO}_4}$ values increase up to +21.1‰ (VCDT), linking the salinity to the migration of groundwater from the surrounding Mesozoic sediments. $^{87}\text{Sr}/^{86}\text{Sr}$ ratios between 0.7108 and 0.7135 and elevated alkali concentrations indicate ongoing water-rock interaction of the evaporite-derived brines with the Carboniferous siliciclastic rocks of the mine. A positive correlation of $^{87}\text{Sr}/^{86}\text{Sr}$ ratios with $\delta^2\text{H}_{\text{H}_2\text{O}}$ and $\delta^{18}\text{O}_{\text{H}_2\text{O}}$ values suggests mixing of the brines with isotopically heavy formation water within the Carboniferous bedrock. The oxidation of pyrite is the dominant sulfate source in shallow mine drainage and groundwater with a relatively low ionic strength ($I < 0.035$), as indicated by $\delta^{34}\text{S}_{\text{SO}_4}$ values between -8.3 and $+0.3\%$ (VCDT). Intermediate water compositions are the result of the dilution of brines with shallow water. In any case, modern meteoric water with $\delta^{18}\text{O}_{\text{H}_2\text{O}}$ values between -6.9 and -8.65% (VSMOW) is the primary water source for brines, groundwater, and mine drainage.

1. Introduction

Coal mine drainage is often characterized by poor water quality, i.e. by low pH values, high concentrations of dissolved toxic metal ions, and high salinity, posing environmental risks for the receiving streams. When groundwater has to be pumped from a mine to allow excavation, this high salinity may become an environmental issue (Banks et al., 1997; Timpano et al., 2015; Turek, 2004), as it may cause toxicity to freshwater communities (e.g. Cañedo-Argüelles et al., 2013; Elphick et al., 2011; Hart et al., 1991). Sulfide mineral weathering can lead to the formation of acid mine drainage solutions (Galán et al., 2003; Neal et al., 2005; Nieto et al., 2007). Low pH (Simate and Ndlovu, 2014) and relatively high sulfate concentrations (Wang et al., 2016) caused by sulfide mineral dissolution may have adverse toxicological effects on freshwater communities. In particular, clogging of the riverbed by the

formation of hydrous ferric oxides has a negative effect on the flora and fauna of the affected rivers (MacCausland and McTammany, 2007; McKnight and Feder, 1984; Scullion and Edwards, 1980). Toxic metal ions are an additional risk for aquatic ecosystems in the receiving water bodies. High loads of dissolved metal ions are often connected to the mining of sulfidic ores. In addition coal mine drainage in several places in Europe (Gombert et al., 2018) or the United States (Cravotta and Brady, 2015) may also carry relevant levels of toxic metals, often related to pyrite oxidation.

A number of passive and active remediation strategies are available, including microbial reduction of sulfate in constructed wetlands, and the addition of lime (Gazea et al., 1996; Johnson and Hallberg, 2005; Wolkersdorfer, 2008). Increasing attention is being devoted not only to avoiding or mitigating the negative environmental effects, but also to recovering and reusing resources deriving from the drainage (Moodley

* Corresponding author.

E-mail address: Thomas.rinder@sbg.ac.at (T. Rinder).

<https://doi.org/10.1016/j.apgeochem.2020.104693>

Received 10 March 2020; Received in revised form 9 July 2020; Accepted 13 July 2020

Available online 31 July 2020

0883-2927/© 2020 The Author(s). Published by Elsevier Ltd. This is an open access article under the CC BY license (<http://creativecommons.org/licenses/by/4.0/>).

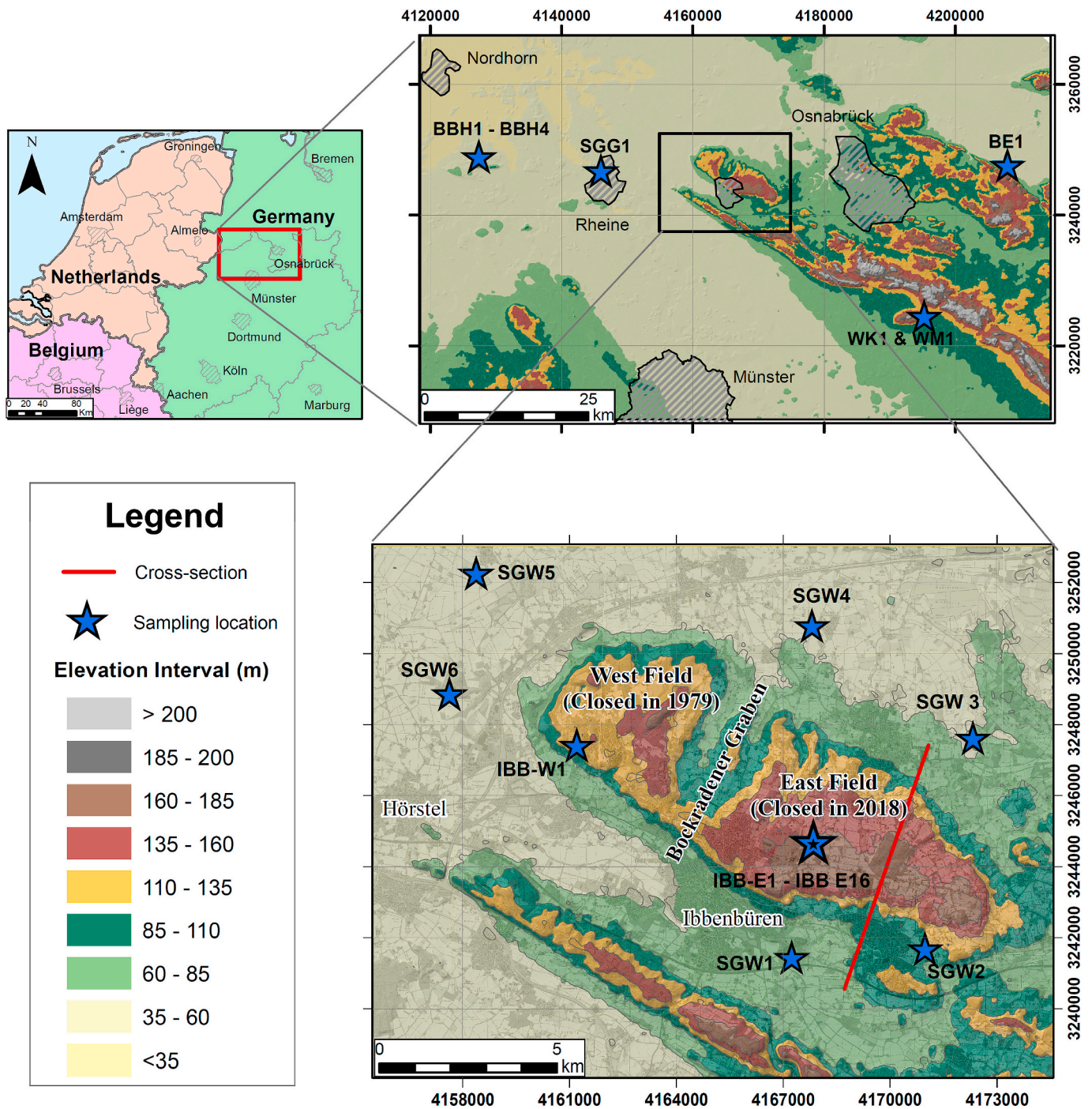


Fig. 1. Location of the Ibbenbüren coalfield. The Carboniferous blocks of the coalfield are divided by faults along the Bockradener Graben. Mining in the Westfield closed in 1979, whereas mining in the Eastfield continued until December 2018. The red line denotes the position of the cross section in Fig. 11. Modified after European Digital Elevation Model (EU-DEM), version 1.1. (For interpretation of the references to color in this figure legend, the reader is referred to the Web version of this article.)

et al., 2018; Naidu et al., 2019; Simate and Ndlovu, 2014). In any case, the design and operation of a suitable remediation process needs to be based on a solid hydrogeochemical model. However, the drainage quality is often predicted solely on the basis of a standard procedure (Dold, 2017; Parbhakar-Fox and Lottermoser, 2015).

Currently, at the anthracite mine in Ibbenbüren, an estimated volume of 15 million m³ of mine drainage enters the receiving stream each year, contributing between 61 and 80% of the total annual chloride load (MKULMV, 2016), frequently exceeding the threshold values considered harmful for freshwater ecosystems. With the mine closure in December

2018, the long-term liabilities related to the discharge of mine drainage from the abandoned mine are in public focus. Currently, the coal mine drainage causes highly saline brines, rich in iron and sulfate. The aim of this study is to examine the relevance of the individual processes of water-rock interaction for the overall chemical composition of the mine drainage solutions. This is essential in order to facilitate the prediction of the future long-term development of the water quality. Towards this goal, a sampling campaign of waters from the active mine as well as the surrounding areas was conducted. Samples were interpreted with respect to main and trace element compositions as well as to the isotope

ratios $^{34}\text{S}/^{32}\text{S}$ and $^{18}\text{O}/^{16}\text{O}$ in sulfate, $^{18}\text{O}/^{16}\text{O}$ and $^2\text{H}/^1\text{H}$ in H_2O , and $^{87}\text{Sr}/^{86}\text{Sr}$ in the dissolved Sr.

On the basis of the acquired data, the dominant reaction mechanisms are identified, and a conceptual model for the chemical evolution of the coal mine drainage solution and the groundwater of the coal mine is developed.

2. Geological setting and sampling location

The first document mentioning the mining of anthracite hard coal from the Ibbenbüren mining region dates back to 1564. In the nearby Piesberg quarry, documents reach further back, to 1461. The cumulative mass of anthracite coal extracted since the beginning of the mining operations is approximately 240 million tons. Historically, the room-and-pillar mining has been an important method. However, since the 1940s, the excavation has been carried out by longwall mining. The depth of the deepest coal seam excavated before the closure of the mine was approximately 1500 m below surface. The mine closed in December 2018 and is now being flooded.

The coalfield, known as the “Ibbenbürener Karbonscholle”, is a horst structure of Carboniferous origin, which was brought up to the surface by uplift in the Cretaceous. As a result, the coalfield is separated from the surrounding area with an offset of up to 2000 m. It consists of two hills (Schafberg and Dickenberg) divided by a NNE-SSW striking graben structure known as the Bockradener Graben (see Fig. 1). The hill chain is surrounded by Triassic, Jurassic, and, to a lesser extent, Permian rock formations in the direct vicinity of the fault structure, surrounding the block. The chain reaches a maximum height of 176 m above sea level, with a length of 14 km and a width of 4–5 km (Bässler, 1970). During mining operations, the Schafberg and Dickenberg were named “Eastfield” and “Westfield”, respectively.

The Carboniferous rocks of the Ibbenbüren coalfield represent the northwesternmost outcrops of the Paleozoic layers in Germany. These layers outcrop again in the Ruhr area, about 90 km South of Ibbenbüren. The slightly north dipping coal seams of the Ruhr area disappear under the sediments of the Münsterland Cretaceous basin to outcrop again in the Ibbenbüren area before being buried under younger sediments in the North German Basin. Although the same coal seams can be identified in both mining regions, the coal produced in Ibbenbüren is classified as anthracite coal. Therefore, it is of significantly higher quality than the hard coal of the Ruhr area. The reason for this higher coalification is still being debated, with two different hypotheses being developed. One theory connects the high coalification to an igneous intrusion in the late Cretaceous, the so-called Bramscher massif. Recently, however, an increasing number of publications suggest that a deep burial during the early Cretaceous seems more likely (Bruns et al., 2013; Bruns and Littke, 2015; Muñoz et al., 2007; Senglaub et al., 2005).

The coal seams within the deposit dip to the North with an angle of 3–25°. The main lithologies are sandstone, siltstone, claystone, and conglomerate. Kaolinite and illite have been reported as the main matrix components in the Pennsylvanian sandstone of the region, which was classified as sub-lithic arenites with low volumes of feldspar grains and muscovite (Wüstefeld et al., 2017). Upper Jurassic halite, gypsum, and anhydrite-bearing formations border with the coalfield and are associated with subsidence phenomena, e.g. the development of sinkholes in the nearby “Heiliges Feld” (Dölling and Strizke, 2009). Halite has also been detected in the Triassic sediments but not in the Permian rocks surrounding the area.

The hydrogeological situation has been discussed in detail, for instance, by Bässler (1970) and Lotze et al. (1962). In general, the Eastfield and the Westfield present different situations, due to the different mining depth as well as to differences in the Quaternary upper layer.

Mining in the Westfield was abandoned in 1979, and flooding was induced. Mining was concentrated close to the surface down to about –170 m below surface, whereas mining in the Eastfield continued to a

depth of approximately –1500 m below surface. Today, the water of the Westfield is entering the Dickenberg gallery (sample IBB-W 1), from where it is brought to a water treatment plant with settling ponds before entering the receiving stream (Ibbenbürener Aa). During active mining, the quantification of the groundwater discharge showed that infiltration from the top of the coalfield alone cannot explain the amount of mine water drainage (Lotze et al., 1962). However, after the rise of the groundwater table above the surrounding aquifers, the inflow from these aquifers can be ruled out (Rudakov et al., 2014).

In the Eastfield, mine water was still pumped at the time of sampling. The mine drainage comprises deep saline brines as well as relatively fresh meteoric waters close to the surface. Mine dewatering is carried out through a central point of discharge from where the water runs through an adit into settling ponds before entering the Ibbenbürener Aa.

Above the Eastfield and the Bockradener Graben, a Quaternary layer of up to 30 m in thickness bears groundwater. Above the Westfield, this layer is less developed; groundwater from this layer was diverted into deeper levels due to mining activities. The same is true for surface streams which are at least periodically water-bearing above the Eastfield but not above the Westfield anymore. Below the first groundwater level, the Carboniferous sandstones themselves form the most important aquifer.

Faults that are striking NNE-SSW through both parts of the coal field often reach into the Mesozoic surrounding areas. They are considered to be important for the regional hydrogeological situation, providing preferential flow paths for water entering into the coal field. The most prominent fault system – the Bockradener Graben – divides Eastfield and Westfield with an offset of up to 510 m (Bässler, 1970). The offset of the faults within the coalfields reaches values of 20–200 m. Historically, large water inflows have been related to fault systems. In general, the faults provide a flow path down to at least –600 to –700 m, where a compressive tectonic regime starts to lower the permeability. Along these faults, meteoric water can easily infiltrate into the mine. In fact, Bässler (1970) noted a temporal correlation of rainfall and discharge of mine drainage. He also noted that together with mining activities, these meteoric waters move down.

The influence of meteoric water was however limited to the upper levels of the mine, and when Bässler (1970) carried out his sampling campaign, the lowest level at that time (–900 m) did not seem to be influenced by meteoric water. With depth, the water discharge was increasingly correlated with mining activities, and was temporarily increasing when the exploitation of new areas led to the outflow of formation water. Bässler (1970) reported a porosity of the sandstones between 15 and 5% together with a permeability generally below 1 mD (millidarcy). While the low permeability of the sandstones would normally inhibit dewatering, the failure of the overburden related to longwall mining creates enough fractures to allow a temporal water-flow. The calculated age of these formation waters based on Tritium and Carbon-14 analyses was >34,000 years in some cases.

3. Methodology

Samples were taken during two different campaigns in summer 2018. Electrical conductivity, dissolved oxygen, temperature, and pH were measured *in-situ* with a WTW 350i multimeter. Redox values were measured with a Lovibond SD60. The German legislation concerning explosion protection in coal mines does not allow the use of electronic devices, so that *in-situ* measurements inside the mine were not possible (solutions IBB-E 1 to IBB-E 16). As a workaround, a gastight bottle (DURAN 150 ml) was used for sampling, and measurements were carried out within 5 h after sampling. All samples were filtered through 0.45 µm regenerated cellulose filters and stored in (i) gastight Duran glass bottles (150 ml) for alkalinity measurements, and (ii) prewashed 125 ml HDPE Nalgene bottles for chemical analyses. Samples for cation analyses were acidified down to pH ≈ 2 with concentrated HNO_3 (Merck ultrapure). The samples were placed in a cooling box and transferred to

the laboratory for measurements. Alkalinity was measured *in-situ* by colorimetry using an Aqualytic AL800 photometer. Ion chromatography and ICP-OES measurements were determined at the Graz University of Technology, Austria. The concentrations of dissolved cations (Na^+ , K^+ , Mg^{2+} , Ca^{2+}) and anions (Cl^- , NO_3^- , SO_4^{2-} and Br^-) were determined by ion chromatography with a Dionex ICS-3000. Chemical analyses of the trace elements were carried out with an ICP-OES (Perking Elmer) with analytical precision better than $\pm 5\%$ based on replicate analyses of the selected samples ($n = 2$). Strontium isotope ratios were determined at the NAWI Graz Central Lab Water, Minerals and Rocks at the Graz University of Technology, Austria. Strontium was separated using a Sr-specific extraction chromatographic resin (Sr spec (T)) using 3 mol l^{-1} HNO_3 . Isotopic ratios were determined on a Plasma 2 MC-ICP-MS (Nu instruments, Wrexham, UK). Measurements were performed with a static cup configuration in wet-plasma mode. Instrumental mass fractionation was corrected for within-run following an exponential law and assuming $^{86}\text{Sr}/^{88}\text{Sr} = 0.1194$. Krypton interferences were corrected for, using a value of $^{86}\text{Kr}/^{84}\text{Kr} = 0.30354$. The baseline was determined prior to each sample analysis for 120 s on-peak, aspirating a blank solution. The reference material NBS 987 was $^{87}\text{Sr}/^{86}\text{Sr} = 0.71026 \pm 0.00002$ (2 SD, $n = 15$). The total procedural blank was $< 0.5 \text{ ng Sr}$ and thus negligible. For analytical details see [Stammeier et al. \(2019\)](#). The isotopic composition of high saline waters was measured by classic isotopic equilibration techniques using the H_2 -water equilibration method for hydrogen ([Horita, 1988](#)) and the CO_2 -water equilibration technique for oxygen ([Epstein and Mayeda, 1953](#)). The IRMS measurements were done with a Finnigan DELTAplus Mass Spectrometer coupled to a fully automated equilibration device adapted from [Horita et al. \(1989\)](#). The isotope values of less mineralized waters were analyzed by wavelength-scanned cavity ring-down spectroscopy (WS-CRDS) using a Picarro L1102-i system. The analytical procedure of the WS-CRDS measurements is similar to that described by [Brand et al. \(2009\)](#). Typical analytical precisions (1σ) were $\pm 1\%$ for $\delta^2\text{H}_{\text{H}_2\text{O}}$ and $\pm 0.08\%$ for $\delta^{18}\text{O}_{\text{H}_2\text{O}}$, and the values were referenced relative to the Vienna Standard Mean Ocean Water (VSMOW). The analysis of $^{34}\text{S}/^{32}\text{S}$ ratios in sulfate was carried out at Imprint Analytics GmbH (Neutal, Austria) using an Eurovector elemental analyzer coupled with a NU Horizon IRMS following the method described in [Révész et al. \(2012\)](#). Measurements were carried out using an in house reference material which was calibrated against IAEA-S-2 with a mean $\delta^{34}\text{S}_{\text{SO}_4}$ of $+22.62 \pm 0.16\%$ and IAEA-S-3 with $-32.49 \pm 0.16\%$. $^{18}\text{O}/^{16}\text{O}$ ratios were determined by the same lab with a Hekatech TCEA coupled to the NU Horizon IRMS. The in house reference material was calibrated against USGS34 and IAEA-NO3 with mean $\delta^{18}\text{O}$ values of $+27.9 \pm 0.6\%$ and $+25.6 \pm 0.4\%$, respectively. The isotopic analyses of sulfur and oxygen in sulfate and hydrogen and oxygen in water were reported in the δ -notation relative to a standard (VCDT for sulfate, V-SMOW for oxygen and hydrogen). Tritium measurements were carried out by liquid scintillation after electrolytic enrichment at Hydroisotop GmbH (Schweitenkirchen, Germany). The computer code PHREEQC ([Parkhurst and Appelo, 1999](#)) with the database wateq.dat was used for hydro-geochemical modelling. For solutions with ionic strength above 1, the thermodynamic calculation was done using the Pitzer.dat database, based on recommendations from [Appelo and Postma \(2005\)](#). Pitzer.dat was also used for calculating seawater evaporation trends in [Fig. 4a to d](#). Depth data herein are given as distances to the highest point of water discharge, i.e. the reference point IBB-E-8. This is the sampling point of cumulative drainage outflow of the Eastfield just before the water reaches the surface, and lies 85 m above normal zero.

4. Results and discussion

4.1. Water types

The 31 sampled solutions cover a wide range of total dissolved solids, from values $< 1000 \text{ mg/kg}$ for the shallow groundwater surrounding the

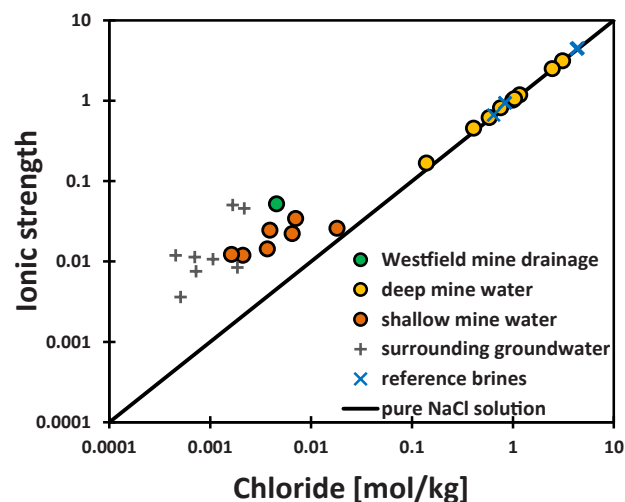


Fig. 2. Chloride concentration [mol/kg] versus ionic strength. Increasing salinity is accompanied by an increasing percentage of sodium chloride in total salinity. The black line represents a pure NaCl (1:1) solution. Solutions plotting above this line indicate a higher fraction of divalent ions contributing to total salinity.

coalfield up to a maximum of 182,000 mg/kg for a brine sample from the deepest levels of the coalfield. Based on these characteristics, the main chemical composition, and the geographical location (see [Fig. 1](#)) of the sampling points, the samples were divided into 5 different types (see [Figs. 2 and 3](#) for identification, and [Table S1](#) (Supplementary Material)). Solution IBB-W 1 (**green circle**) was sampled at the surface from the Dickenberg gallery, which gathers all groundwater from the flooded Westfield and is now the only effluent of the mine water from this part of the coalfield. The water type is classified as Ca-Mg-Na-SO₄ (see [Table S1](#) (Supplementary Material)). Additionally, the mine drainage at this point is characterized by high loads of dissolved and particulate iron. The solutions from the coalfield sampled from depths below the third level ($\approx -270 \text{ m}$) are all characterized by a relatively high ionic strength (> 0.1) and are of Na-Cl water type (IBB-E 1 to IBB-E 9; **yellow circles**). This group also includes solution IBB-E 8, whose high salinity does not correspond to the depth of the sampling point. IBB-E 8 was taken from the main drainage of the Eastfield, just before reaching the surface. It represents therefore a mixture of all the waters which are pumped from the mine, including the deep brines. Waters sampled down to the third level ($\approx -270 \text{ m}$) (IBB-E 10 to IBB-E 16; **orange circles**) are characterized by relatively low ionic strength. A water type cannot be assigned to this group, as the waters show highly variable contents of the main cations (calcium, sodium, and magnesium) with an anionic dominance of sulfate, bicarbonate, and chloride. The high fraction of divalent ions contributing to the ionic strength is shown in [Fig. 2](#). The water type plots above the black line, representing a pure NaCl solution.

For comparison, saline waters originating from other hydro-geological settings (**blue X marks**) in the wider surroundings of the coalfield were sampled and analyzed. All of them can be characterized as belonging to the Na-Cl water type. These samples include the groundwater, originating from two wells drilled into lower Triassic sediments, used for the thermal spa in Bad Bentheim (BBH 1 and BBH 2), as well as three samples from the Northern border of the Münsterland Cretaceous Basin, originating from two wells drilled into Cretaceous sediments in the city of Bad Rothenfelde (WK 1 and WM 1), and a sample from the well of the Saline Gottesgabe saltworks in the city of Rheine (SGG 1). One sample was taken from a well drilled in the North German Basin close to the city of Bad Essen (BE 1). The last group constitutes the shallow groundwater (**grey crosses**) surrounding the coalfield (SGW 1 to SGW 6), as well as two shallow groundwaters originating from an aquifer of Upper Jurassic sediments, which are used for the thermal spa

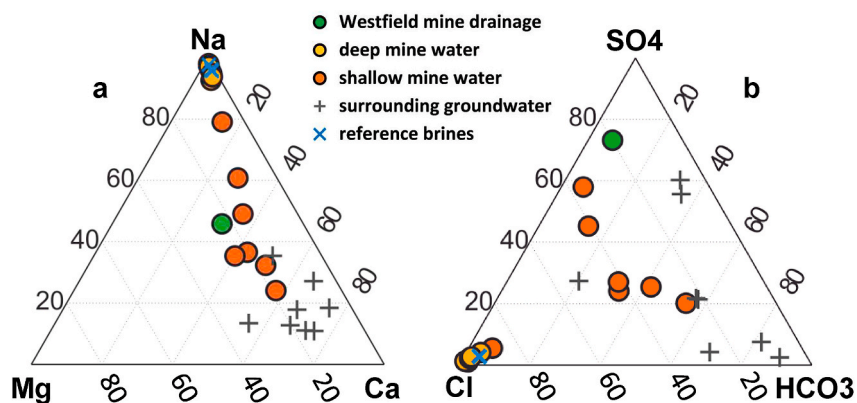


Fig. 3. Ternary plots showing the relative molar proportion of main cations (Mg^{2+} , Ca^{2+} , and Na^+) (a), and main anions (SO_4^{2-} , Cl^- , and HCO_3^-) (b).

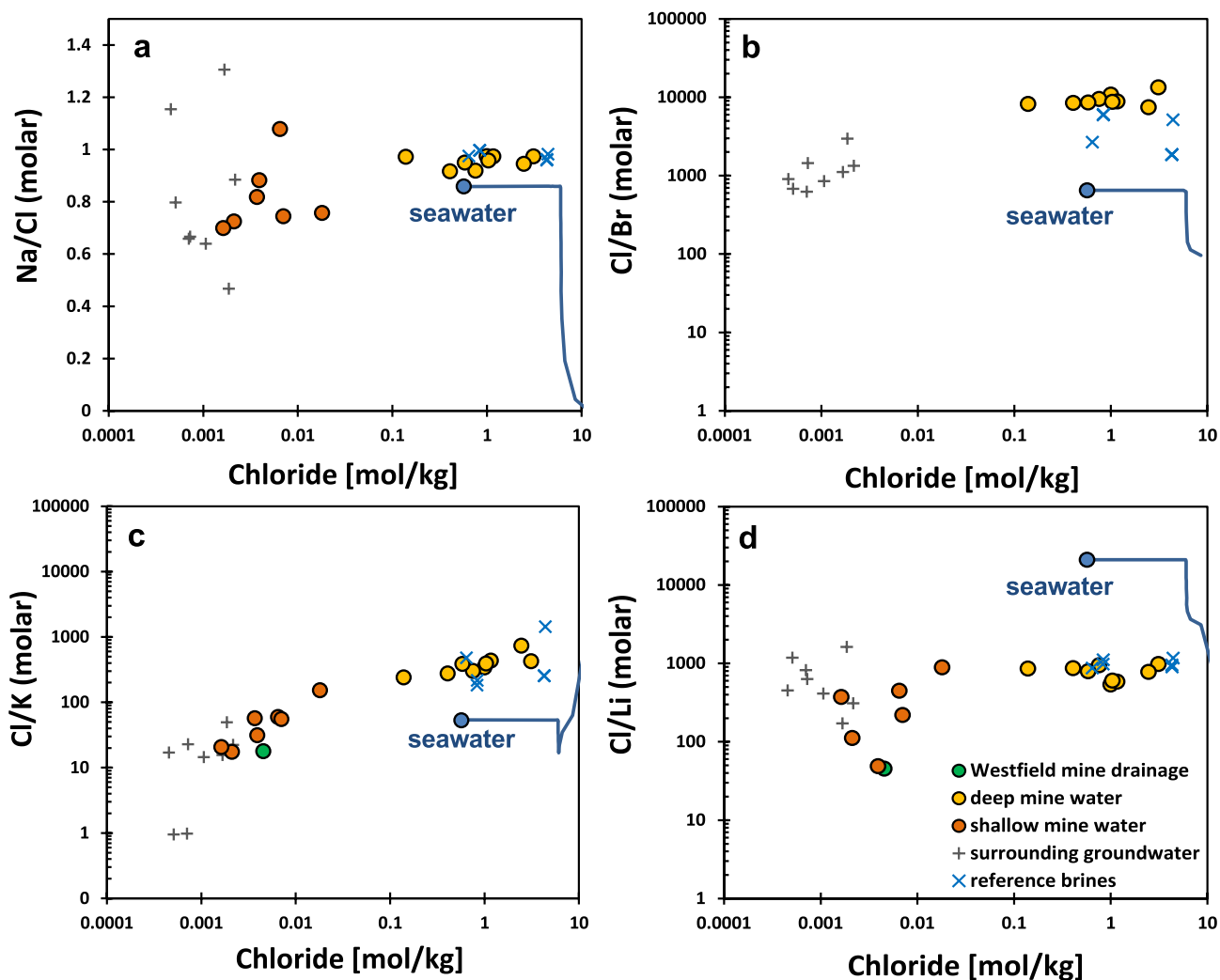


Fig. 4. Molar Na/Cl (a), Cl/Br (b), Cl/K (c), and Cl/Li (d) ratios versus Cl concentration [mol/kg]. Seawater composition after [Millero et al. \(2008\)](#); Lithium concentration taken from [Riley and Tongudai \(1964\)](#); Evolution of the respective molar ratio during seawater evaporation until saturation of carnallite is reached for comparison (blue line). (For interpretation of the references to color in this figure legend, the reader is referred to the Web version of this article.)

in Bad Bentheim (BBH 3 and BBH 4). As those waters originate from different geological units, they are characterized by diverse contents of main ions. In any case, however, Ca^{2+} is the dominant cation (see [Fig. 3](#) and [Table S1](#) (Supplementary Material)).

4.2. Geochemical evolution and reaction mechanisms

4.2.1. Dissolution of evaporites from adjacent layers

The chemical composition of the analyzed water is summarized in [Table S1](#) (Supplementary Material). The chloride concentration in the deep mine water (IBB-E 1 to IBB-E 9) is between 7.6 and 1910 times

higher than that of the corresponding shallow mine water down to the third level. The strong correlation of Na^+ versus Cl^- points to halite dissolution as the main source of salinity in these waters (see Figs. 2 and 4a). The Cl/Br ratio in the solutions from the coalfield is relatively constant (see Fig. 4b), indicating a single source of salinity for both elements. Note that the Br^- concentration in sample IBB-W 1 and in the shallow mine waters (IBB-E 10 to IBB-E 16) was below the detection limit.

The Na/Cl ratios indicate that a single source of salinity starts to influence the mine water chemistry below the third level (≈ -270 m). There is no indication of halite dissolution in the shallow waters above. Note that, while indicating halite dissolution as the main source of Na^+ , the deep mine waters show a Na^+ depletion with respect to Cl^- (see Table S1 (Supplementary Material) for Na/Cl ratios). A loose correlation between the decreasing Ca^{2+} content and the increasing Na/Cl ratio suggests a Na^+ source/ Ca^{2+} sink mechanism similar to the observations of Kloppmann et al. (2001). Cation exchange of the saline waters with clay minerals in the siliciclastic aquifer is a plausible explanation for this trend.

The observed Cl/Br ratios (between 13,457 and 7,465) are well within the expected values for halite dissolution and further corroborate the impression gained from Na/Cl ratios.

In general, Cl/Br ratios have been used to evaluate the origin of salinity in various hydrogeological settings (e.g. Alcalá and Custodio, 2008; Chowdhury et al., 2018; Davis et al., 1998; Egeberg and Aagaard, 1989; Fontes and Matray, 1993a; Katz et al., 2011; Kloppmann et al., 2001; Panno et al., 2006). Those studies took advantage of the relatively conservative behavior of Cl^- and Br^- in most aquatic environments, which allows to use those ions to trace the origin of groundwater salinity. During halite formation, bromide will co-precipitate with halite (Braitsch and Herrmann, 1963; McCaffrey et al., 1987; Siemann and Schramm, 2000). This co-precipitation can be followed using the distribution coefficient after McCaffrey et al. (1987):

$$D_{\text{Br}^-} = \frac{[\text{Br}^-]/[\text{Cl}^-]_{\text{halite}}}{[\text{Br}^-]/[\text{Cl}^-]_{\text{brine}}} \quad (1)$$

The average D_{Br^-} found by these authors is rather constant around 0.032. The molar Cl/Br of modern seawater is around 650. This ratio is suggested to have been constant throughout Earth's history (Fiori et al., 2004; Horita et al., 2002, 1991). On a local scale, upon evaporation of seawater, this ratio will decrease with the onset of halite precipitation and reach a value around 40 in the late evaporation stage at the onset of carnallite ($\text{KMgCl}_3 \cdot 6\text{H}_2\text{O}$) precipitation. Therefore, the Br^- concentration of halite formed during an early evaporation stage concentration will be lower compared to later evaporation stages, following a Rayleigh fractionation pattern as the solution gets enriched in Br^- relative to Cl^- . The Cl/Br ratio at the initial start of halite precipitation will be approximately 20,000, and will lower to about 5,500 in the halite, i.e. well within the range of 13,457 to 7,465 observed in the Ibbenbüren brines. Minerals like carnallite and sylvite incorporate Br^- into the crystal structure more readily compared to halite (Hardie and Eugster, 1971), so the influence of the respective minerals is not evident.

4.2.2. The interaction of brines with the carboniferous bedrock

The incorporation of K^+ into halite during seawater evaporation can be described by equation (2):

$$D_{\text{K}^+} = \frac{[\text{K}^+]/[\text{Na}^+]_{\text{halite}}}{[\text{K}^+]/[\text{Na}^+]_{\text{brine}}} \quad (2)$$

According to McCaffrey et al. (1987), D_{K^+} averages to 0.0008, which corresponds to a Na/K ratio in halite between 5,000 in the early evaporation stage and 2,000 at later stages. The Na/K ratio of deep mine waters is between 235 and 700. According to equation (2), if all Na^+ in the analyzed solutions is attributed to halite, the dissolution of halite may account for 19 up to a maximum of 56% of K^+ in the deep mine

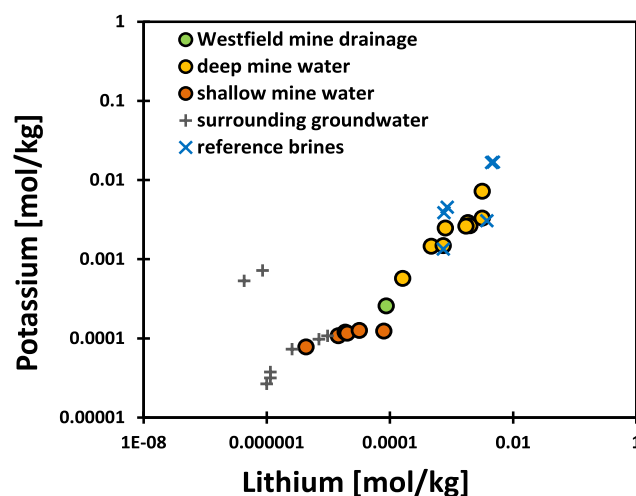


Fig. 5. Lithium concentration versus potassium concentration [mol/kg].

waters (IBB-E 1 to IBB-E 10). The K^+ concentration of the shallow mine waters is rather constant and explains at most 5% of the total K^+ concentration of deep waters. Consequently, an additional source of K^+ other than halite is needed to explain the observed values. In principle, further possible sources of K^+ in the groundwater are:

- (1) K^+ -rich evaporites like carnallite or sylvite from the surrounding area;
- (2) K-feldspar, muscovite, and clay minerals from the matrix of the Carboniferous sandstone;
- (3) fertilizers.

(1) Evaporites with high K^+ content have not been reported in the Mesozoic rocks surrounding the study area. The only sources of such minerals are the Permian sedimentary rocks of the Zechstein unit, which once covered the coalfield. The Permian Zechstein Sea is known to have reached the evaporation stage for carnallite in some areas of Germany. Therefore, the formation water, which originates from the dissolution of such Permian evaporites, might produce elevated K^+ contents. However, to our knowledge, no carnallite or sylvite has been reported in the Zechstein deposits surrounding the coalfield, and the contribution of carnallite or sylvite dissolution is not evident from the Cl/Br ratios. Additionally, $\delta^{34}\text{S}_{\text{SO}_4}$ values of the dissolved sulfate (see chapter 4.3.3) do not indicate the contribution of Permian deposits.

(2) K^+ concentrations not only show a strong correlation with chloride (see Fig. 4c), but also with Li concentrations (see Fig. 5). A strong positive correlation of K^+ and Li^+ suggests aluminosilicates as the source of these elements. The origin of Lithium from the dissolution of evaporites seems unlikely due to a very limited uptake of Li in either halite or any other minerals of the evaporation series (e.g. Fontes and Matray, 1993a; Shalev et al., 2018). Evaporation of seawater generates elevated Cl/Li ratios compared to the mine waters (see Fig. 4d). This is a frequent observation for saline brines, in which Li concentrations readily exceed the sea water composition as well as concentrations that might be reached during evaporation of such seawater (Chan et al., 2002; Stueber et al., 1993). The interaction of the mine water with aluminosilicates in the aquifer is a likely source in this case.

Fractured and porous sandstone with low volumes of feldspar and muscovite is the main aquifer of the Ibbenbüren coalfield. Illite has been reported as an important matrix component within this sandstone (Becker et al., 2017; Wüstefeld et al., 2017), with kaolinite as a minor component. From thermodynamic considerations, the dissolution of illite or feldspar at current ambient temperature conditions cannot generate the observed K^+ concentrations (Zhu, 2005). In accordance

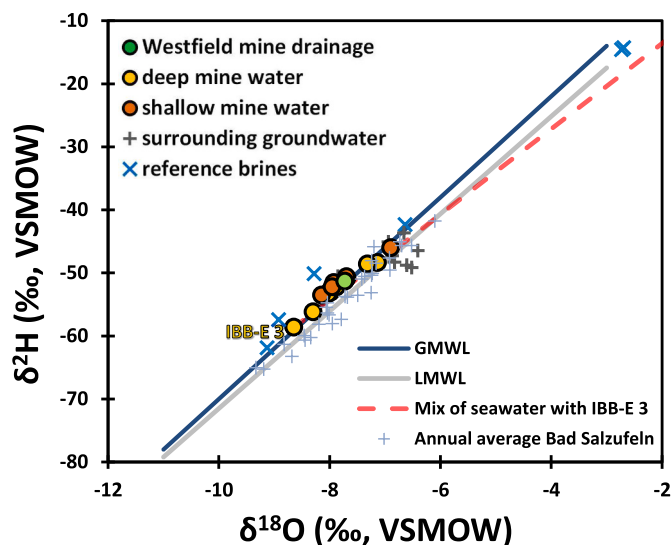
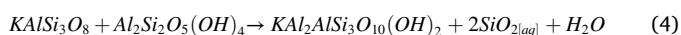
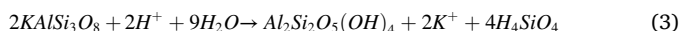


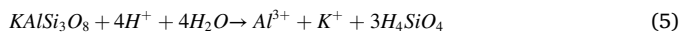
Fig. 6. $\delta^{18}\text{O}$ versus $\delta^2\text{H}$ values (‰; VSMOW). The blue line denotes the Global Meteoric Waterline (GMWL) after Craig (1961). The grey line denotes the Local Meteoric Waterline (LMWL) of the nearest station (Bad Salzufen) obtained from the IAE/WMO global network of isotopes in precipitation (GNIP) database Stumpp et al. (2014). Light grey crosses are annual average values of the station from 1978 to 2011, plotted for reference. The red dotted line shows the hypothetical trend during mixing of solution IBB-E 3 with seawater. (For interpretation of the references to color in this figure legend, the reader is referred to the Web version of this article.)

with the respective mineralogy, other processes that influence the K^+ content in solution include kaolinite formation and illitisation (Egeberg and Aagaard, 1989).

Incongruent dissolution of K-feldspar and subsequent kaolinite formation are accompanied by the liberation of K^+ ions, as represented by equation (3). The subsequent illitisation of kaolinite in equation (4) after Thyne et al. (2001) would remove K^+ from the solution again. However, the formation of illite according to equation (4) in the investigated setting occurs only in a temperature window from around 70 °C up to around 130 °C (Becker et al., 2017).



Outside this temperature window, the reaction will not be completed. A decrease in K^+ and aluminum contents due to the dissolution of k-feldspar under open system conditions has been reported in other sandstone reservoirs (Ehrenberg, 1991; Wilkinson et al., 2014), following equation (5).



It can be hypothesized that the resulting K^+ might be preserved in formation water. K^+ might also be adsorbed onto clay minerals in general, being available for ion exchange reactions at later stages (e.g. Thyne et al., 2001; Wilkinson et al., 2014). Ion exchange of K^+ from the interlayer of illite in the presence of sodium has been reported by Scott and Smith (1966). Bibi et al. (2011) reported an increasing release of K^+ with increasing salinity for experiments carried out with illite at different pH values and two different ionic strengths.

(3) The influence of agriculture seems negligible for most water samples and especially for the mine waters. The measured K^+ concentrations in the shallow mine waters are in the range of the normal background expected for groundwater in the area (Wendland et al., 2005). This holds true notwithstanding ionic strength values that are elevated with respect to the local shallow groundwater (SGW 1 to SGW 6). Other ions indicative of fertilizers such as nitrate or phosphate were

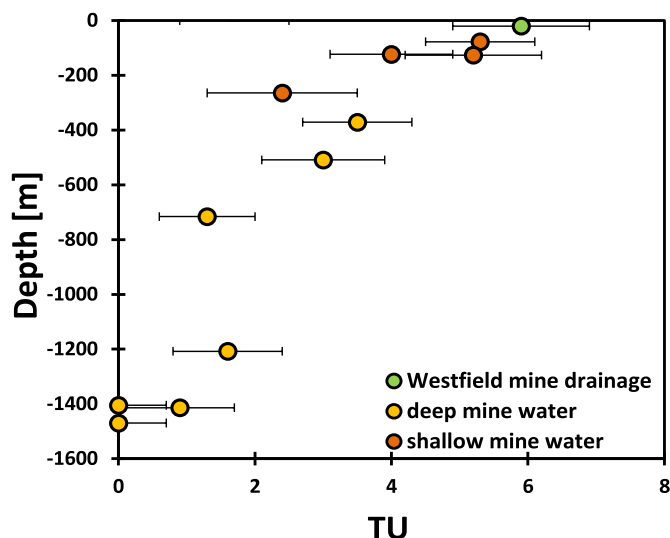


Fig. 7. Tritium units (TU) versus depth in meters. Within the uncertainty, Tritium was present down to the lowest level, indicating the presence of some modern water throughout the mine. Samples IBB-E 3 and IBB-E 4 from the lowest level show TU values below the detection limit (<0.6 TU). Tritium was not analyzed in all samples (see Table S1 (Supplementary Material)).

only found in SGW 3 and SGW 4, taken from agricultural areas surrounding the coalfield. In the latter case, the influence of manure and fertilizer might play a distinctive role in the formation of the waters, but a detailed interpretation of the underlying mechanisms is outside the scope of this article.

4.3. Isotopic signatures

4.3.1. Deuterium and oxygen

The shallow groundwater samples of the surrounding aquifers (SGW 1–SGW 6) plot in the field of the local meteoric precipitation, but with a low d-excess compared to the LMWL (local meteoric water line; see Fig. 6). The summer of 2018 was extraordinarily dry and warm compared to the average climate situation. The shallow groundwater also plots in the upper, isotopically heavy area compared to the annual composition of precipitation in the area (light grey crosses). We therefore assume that the shallow groundwater in this region shows signals of evaporation. Compared to the LMWL, the mine waters of the coalfield show a slight offset towards the GMWL. Such a relatively high d-excess compared to the LMWL might indicate a high proportion of autumn and winter rain events. The average annual precipitation in the area is rather constant through the year, with small maxima from July to September and from December to January. A high d-excess is generally related to relatively low humidity over the oceans (e.g. Pfahl and Sodemann, 2014), which is the case during autumn and winter in the North Atlantic ocean. Evapotranspiration losses above the coalfield, which is under extensive agricultural use, should result in an overrepresentation of precipitation from late autumn and winter within the aquifer.

There is no correlation of the isotopic ratios with depth. Neither influence of Pleistocene waters nor mixing of meteoric water with formation waters of oceanic origin can be deduced from these values. Isotopic evolution during mixing of meteoric water with formation water of oceanic origin is indicated in Fig. 6 (red dashed line). Pleistocene waters show signals that are isotopically light, compared to our values (e.g. Kloppmann et al., 2001). Additionally, Tritium is present in solutions from all levels of the mine down to ≈ -1500 m. Samples BBH 1 and BBH 2 show an isotopic composition typical of precipitation under warmer climate conditions, rather than a mix of meteoric water with seawater or evaporating brines (e.g. Knauth and Beeunas, 1986).

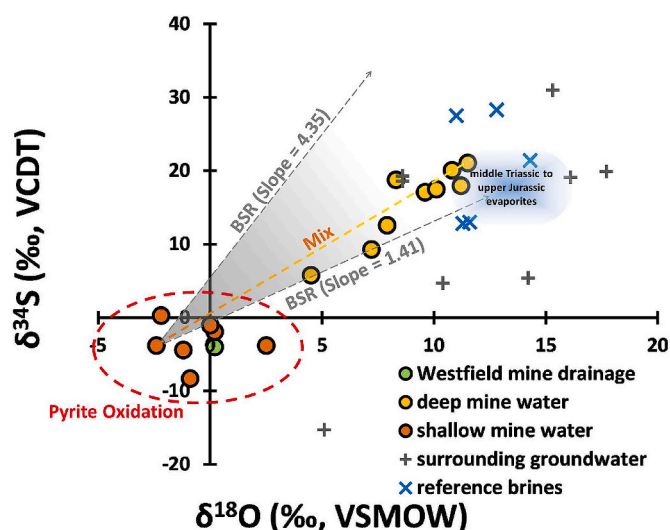


Fig. 8. $\delta^{34}\text{S}$ versus $\delta^{18}\text{O}$ (‰, VCDT) values of dissolved sulfate. The area between the dashed grey lines indicates the possible pathways of isotopic evolution during bacterial sulfate reduction (BSR), starting from sample IBB-E-14; slopes are derived from Brunner et al. (2005). The isotopic trend during conservative mixing is indicated for endmember IBB-E-3 (highest $\delta^{34}\text{S}$, highest ionic strength) with IBB-E-14 (pyrite oxidation, high sulfate). $\delta^{34}\text{S}$ range for middle Triassic to upper Jurassic evaporites from Müller et al. (1966), the range of $\delta^{18}\text{O}$ is based on Claypool et al. (1980).

4.3.2. Tritium

Tritium (^3H) is the radioactive isotope of hydrogen with a half-life of ≈ 12.4 years. It is reported in tritium units (TU), where 1 TU equals 1 ^3H atom in 10^{18} atoms of hydrogen (Kendall and Doctor, 2003). Natural background levels of Tritium are between 1 and 10, but significant amounts of Tritium have been emitted into the atmosphere during nuclear bomb tests in the '50s and '60s. The quantification of Tritium does not allow to calculate the groundwater age as the measurement of its decay product (^3He) would be needed as well (e.g. Schlosser et al., 1988). However, the presence of Tritium implies the presence of some fraction of modern (i.e. after 1950s) water. Tritium has been measured in 13 solutions from the coalfield. Tritium data indicate an increasing groundwater age with depth (Fig. 7). Tritium is present down to the lowest level, approximately 1500 m below the surface. Note that the solutions IBB-E 3 and IBB-E 4 from the lowest level are free of Tritium within uncertainty. However, $\delta^2\text{H}_{\text{H}_2\text{O}}$ and $\delta^{18}\text{O}_{\text{H}_2\text{O}}$ values do not indicate the contribution of formation water as the main mechanism determining the chemical composition of the water. On the contrary, it seems likely that ongoing water rock interaction is contributing to the formation also of the saline brines, which are influenced by meteoric water infiltration.

4.3.3. Sulfur and oxygen in sulfate

The interpretation of sulfur and oxygen isotopes in sulfate is based on the groundbreaking work carried out by Claypool et al. (1980), Holser and Kaplan (1966), and Müller et al. (1966) showing that the sulfur and oxygen isotopic composition of seawater sulfate changed through time. Since those seminal works, numerous measurements have helped to improve our knowledge about temporal and spatial patterns of the record preserved (e.g. Bernasconi et al., 2017; Kampschulte and Strauss, 2004; Strauss, 1997; Turchyn and Schrag, 2006; Utrilla et al., 1992). The role of microbes in the sulfur cycle and the traces they leave in the isotopic signal has been thoroughly investigated (e.g. Balci et al., 2007; Böttcher et al., 2001; Habicht and Canfield, 1997). The isotopic signals have proven useful to trace the origin of sulfur in various hydrogeological settings (Bottrell et al., 2008; Brenot et al., 2015, 2007; Burke et al., 2018; Dogramaci et al., 2001; Fontes and Matray, 1993b; Otero

and Soler, 2002; Tichomirowa et al., 2010), and specifically within the context of mine drainage (Gammons et al., 2013; Migaszewski et al., 2018). The sample distribution in Fig. 8 points to different sources of dissolved sulfate. Shallow mine waters (IBB-E 10 to IBB-E 16; IBB-W 1) show a $\delta^{34}\text{S}_{\text{SO}_4}$ signature between -8.3‰ and $+0.3\text{‰}$ with $\delta^{18}\text{O}_{\text{SO}_4}$ values between -2.4 and $+2.5\text{‰}$. In contrast, the deep mine waters (IBB-E 1 to IBB-E 9) are isotopically heavy with $\delta^{34}\text{S}_{\text{SO}_4}$ values between $+5.8$ and $+21.1\text{‰}$, and $\delta^{18}\text{O}_{\text{SO}_4}$ ranging from $+4.5$ to $+11.2\text{‰}$. The isotopic composition of the shallow mine waters (IBB-E 10 – IBB-E 16; IBB-W 1) is typical for sulfate derived from oxidation of pyrite (e.g. Brenot et al., 2015; Haubrich and Tichomirowa, 2002).

For sulfate derived from pyrite oxidation, the $\delta^{18}\text{O}_{\text{SO}_4}$ values can be used to decipher the oxidation mechanism (e.g. Balci et al., 2007; HeideI et al., 2013, 2011, and references therein). In principle, the oxidation of pyrite can utilize O_2 or Fe(III) as oxidant. If Fe(III) is the oxidant, then the oxygen in the newly formed sulfate will derive mainly from H_2O . Both sources will have a different isotopic fingerprint, with the H_2O -derived oxygen being relatively light compared to the O_2 -derived oxygen. $\delta^{18}\text{O}_{\text{H}_2\text{O}}$ of the Ibbenbüren groundwaters is $\approx -8\text{‰}$. The isotope enrichment factor between sulfate and water during pyrite oxidation $\epsilon_{\text{SO}_4-\text{H}_2\text{O}}$ ($\epsilon_{\text{SO}_4-\text{H}_2\text{O}} \approx \delta^{18}\text{O}_{\text{SO}_4} - \delta^{18}\text{O}_{\text{H}_2\text{O}}$) has been reported to be between 0 and 4‰. Accordingly, if H_2O is the sole source of oxygen in sulfate, then the $\delta^{18}\text{O}_{\text{SO}_4}$ should be between -4 and -8‰ . In contrast, the $\delta^{18}\text{O}_{\text{O}_2}$ of the atmospheric oxygen is $\approx +23.5\text{‰}$. The isotopic enrichment factor between sulfate and atmospheric oxygen during pyrite oxidation $\epsilon_{\text{SO}_4-\text{O}_2}$ ($\epsilon_{\text{SO}_4-\text{O}_2} \approx \delta^{18}\text{O}_{\text{SO}_4} - \delta^{18}\text{O}_{\text{O}_2}$) has been reported to be between -4.3 and -9.8‰ (Heidel and Tichomirowa, 2011). Accordingly, if O_2 is the sole source of oxygen in sulfate, then the $\delta^{18}\text{O}_{\text{SO}_4}$ should be between $+13.7$ and $+19.2\text{‰}$. In the studied waters, the $\delta^{18}\text{O}_{\text{SO}_4}$ values between -2.4 and $+2.5\text{‰}$ suggest the oxidation of pyrite through Fe(III) as the main oxidant. Finally, the denitrification of nitrate could also contribute to pyrite oxidation in an agricultural area (Böttcher et al., 1990; Zhang et al., 2009).

With the depth increasing, sulfate becomes increasingly isotopically heavy for both sulfur and oxygen. Two different mechanisms have to be considered to explain this trend of isotopic enrichment, as detailed below.

- (1) Processes that influence the isotopic composition of sulfur and oxygen in sulfate include microbial sulfate reduction and sulfur disproportionation (Antler et al., 2013; Böttcher et al., 2001; Taylor et al., 1984; Thamdrup et al., 1993). A maximum isotope fractionation between sulfate and hydrogen sulfide of $\delta^{34}\text{S}_{\text{SO}_4 - \text{H}_2\text{S}} \approx -70\text{‰}$ has been reported during bacterial sulfate reduction (e.g. Brunner et al., 2005). BäSSLER (1970) proposed bacterial sulfate reduction as the reason for the increasingly heavy $\delta^{34}\text{S}_{\text{SO}_4}$ and $\delta^{18}\text{O}_{\text{SO}_4}$ values of the remaining sulfate in the Ibbenbüren Eastfield. A closer investigation of this hypothesis is of relevance for the setup of a conceptual hydrogeological model, as for this reason the author concluded that the influence of the infiltration of water from the Mesozoic sediments outside of the coalfield is negligible.
- (2) The isotopic composition of sulfate from the dissolution of Mesozoic sediments surrounding the coalfield results in an isotopic signature as is found in the deep mine waters. Comparable $\delta^{34}\text{S}_{\text{SO}_4}$ values around $+20\text{‰}$ for upper Jurassic and middle Triassic gypsum and anhydrite have been reported by Müller et al. (1966). The apparent trend could be caused by the mixing of two endmembers: (i) meteoric water with an isotopic signature derived from pyrite oxidation, and (ii) brines with signatures derived from dissolution of evaporates from the vicinity of the coal field.

The expected isotopic evolution for both scenarios is examined in Fig. 8. The chosen endmembers for the “mixing hypothesis” are solution IBB-E 3 (highest ionic strength and highest $\delta^{34}\text{S}_{\text{SO}_4}$) for the dissolution of

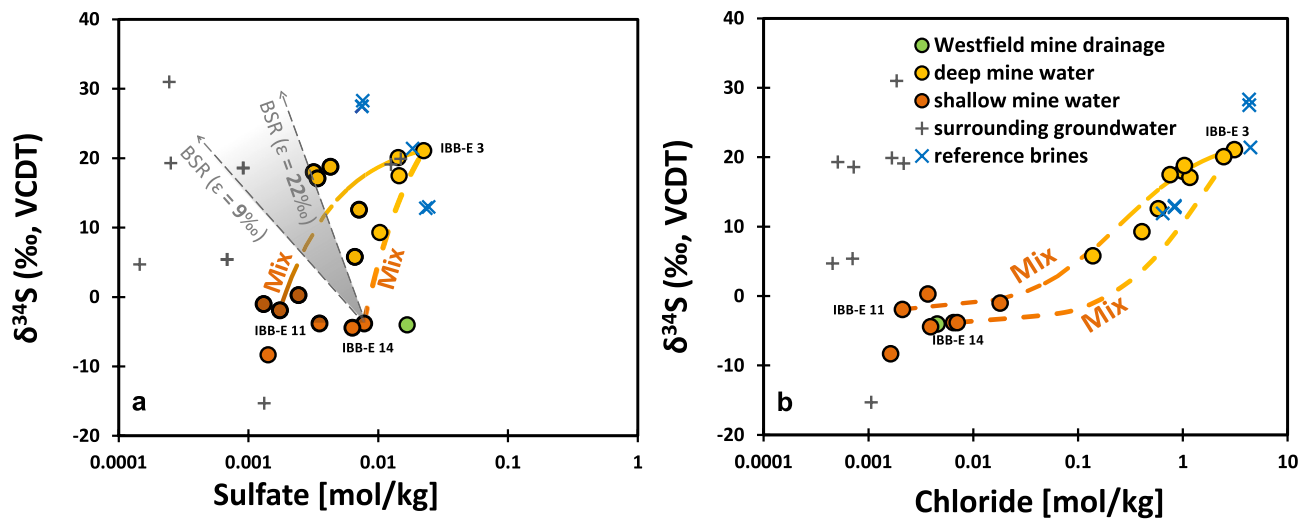


Fig. 9. $\delta^{34}\text{S}$ versus dissolved sulfate (a) and $\delta^{34}\text{S}$ versus chloride [mol/kg] (b). The area between the dashed grey lines denotes isotopic enrichment (ϵ) during bacterial sulfate reduction (BSR). The slopes are derived from Fritz et al. (1989). Endmember mixing is plotted for solution IBB-E 3 with IBB-E 14 (high sulfate), and for IBB-E 3 with IBB-E 11 (low sulfate).

Mesozoic evaporites, and IBB-E 14 as the pyrite endmember with a typical isotopic signature for pyrite oxidation. In principle, the mixing of those two endmembers delivers a plausible fit for most of the analyzed waters. However, the samples are also within the expected trend for the isotopic evolution of the pyrite endmember during bacterial sulfate reduction.

Investigating the correlation of $\delta^{34}\text{S}_{\text{SO}_4}$ against the dissolved sulfate reveals that, on average, sulfate in the deep mine waters is higher compared to the shallow mine waters (see Fig. 9a). Therefore, if bacterial sulfate reduction (BSR) or disproportionation is the dominant process leading to isotopic enrichment in the deep brines, an additional source of sulfur during infiltration is needed. Sedimentary pyrite and sulfur from the coal are possible sources of additional sulfate in this case. A source of isotopically heavy values is the coal derived sulfur, for which values from approximately -50% to $+40\%$ have been measured (Seal, 2006). High isotopic ratios of pyrite have also been reported by Drake et al. (2018), but commonly sedimentary pyrite is isotopically light with respect to the initial sulfate (Strauss, 1997), with more common values being slightly negative or circumneutral. Three pyrite samples measured from the Ibbenbüren coalfield range from $\delta^{34}\text{S}_{\text{FeS}} = -4$ to $+8\%$ (Bässler, 1970). Bernardez et al. (2013) carried out batch experiments to investigate the influence of sulfate concentration on the conversion rate of sulfate to H_2S in the presence of sulfate reducing bacteria. They found an increasing conversion rate of sulfate to H_2S with increasing sulfate content. On that account, it is doubtful whether a system can be under the influence of BSR and at the same time sulfate can be increasing with depth. However, the sample distribution in Fig. 9a would need such a process. Additionally, while sulfate reducing bacteria have been reported at very high salinities (Foti et al., 2007), the salinity of the brines IBB-E 3 and IBB-E 4 is so high that some limitations regarding the possible mechanisms of microbial sulfate reduction have to be considered (Oren, 1999).

However, solutions IBB-E 1, IBB-E 2, and IBB-E 9 are in the range of BSR starting from pyrite endmember IBB-E 14 (see Fig. 9a).

The expected isotopic fractionation of the pyrite endmember during BSR is described using the Rayleigh equation (6), for which kinetic isotope enrichment factors have been described by Fritz et al. (1989).

$$\delta^{34}\text{S}_{\text{remaining sulfate}} = \delta^{34}\text{S}_{\text{init}} - \epsilon^{34}\text{S}_{\text{BSR}} \cdot \ln f \quad (6)$$

where f is the fraction of the remaining sulfate, $\delta^{34}\text{S}_{\text{init}}$ is the $\delta^{34}\text{S}_{\text{SO}_4}$ composition of the initial sulfate, and $\epsilon^{34}\text{S}_{\text{BSR}}$ is the kinetic isotope enrichment factor expressed in ‰ (see, e.g. Hayes (2004) for details

about notation). The $\epsilon^{34}\text{S}_{\text{BSR}}$ found by these authors is between 9% and 22%. The $\delta^{34}\text{S}_{\text{init}}$ value of the “pyrite endmember” IBB-E14 is -3.8% . BSR would create solutions with lower dissolved sulfate content at the respective $\delta^{34}\text{S}_{\text{SO}_4}$ values for most solutions. Applying a large kinetic enrichment factor of 22% and starting from a solution rich in dissolved sulfate (IBB-E 14), the isotopic composition and amount of dissolved sulfate can be reached for solutions IBB-E 1, IBB-E 2, and IBB-E 9. The rest of the intermediate solutions can be described through mixing of the brine endmember (IBB-E 3) and pyrite-derived solutions with high (IBB-E 14) or low dissolved sulfate content (IBB-E 11). However, $\delta^{34}\text{S}_{\text{SO}_4}$ values also increase with salinity. The isotopic composition of sulfate resulting from the dissolution of Mesozoic sediments surrounding the coalfield could result in an isotopic signature as that found in the deep mine waters. This possibility is corroborated by a correlation of increasing $\delta^{34}\text{S}_{\text{SO}_4}$ with an increase in dissolved chloride (see Fig. 9b). The coevolution of $\delta^{34}\text{S}_{\text{SO}_4}$ together with increasing Cl^- concentrations can be described through endmember mixing, according to the sulfate concentration of the pyrite endmember. The mixing of IBB-E 14 (high sulfate concentration) with the brine (IBB-E 3) produces solutions that are isotopically light with respect to the observed values. Some influence of BSR is suggested in that case in accordance with the modelling result shown in Fig. 9a. However, the mixing of solution IBB-E 11 (low sulfate concentration) with the brine (IBB-E 3) generally fits well with the observed trend. Conclusively, the intermediate waters seem to be mostly influenced by the mixing of two endmembers. BSR cannot be fully excluded and might contribute to the observed isotopic evolution with depth but in any case mixing will be the governing process.

Finally, some of the reference samples were taken from defined geological systems. Therefore, BBH 1 and BBH 2 were gathered from an aquifer of Buntsandstein with $\delta^{34}\text{S}_{\text{SO}_4}$ values between $+27.5$ and $+28.3\%$. High values for lower Triassic sediments have been reported, e.g., by Kampschulte and Strauss (2004). The origin of SGG 1 is under debate, but a $\delta^{34}\text{S}_{\text{SO}_4}$ value of $+11.9\%$ is indicative of Permian origin. WM 1 and WK 1 were sampled from the sediments of the Münsterland Cretaceous basin. The origin of the salinity in these waters is not clear, but the values indicate Permian origin. From Fig. 9b, it should be considered, however, that a mixture of pyrite dissolution and evaporate in analogy to the mine waters could also be responsible for the observed $\delta^{34}\text{S}_{\text{SO}_4}$. The $\delta^{34}\text{S}_{\text{SO}_4}$ values of sulfate in atmospheric deposition in Central Europe vary between 0% and $+7\%$, whereas $\delta^{18}\text{O}_{\text{SO}_4}$ values range between $+7\%$ and $+17\%$ (Knöller et al., 2004; Novák et al., 2001), which would be indicative of the isotopic composition of samples

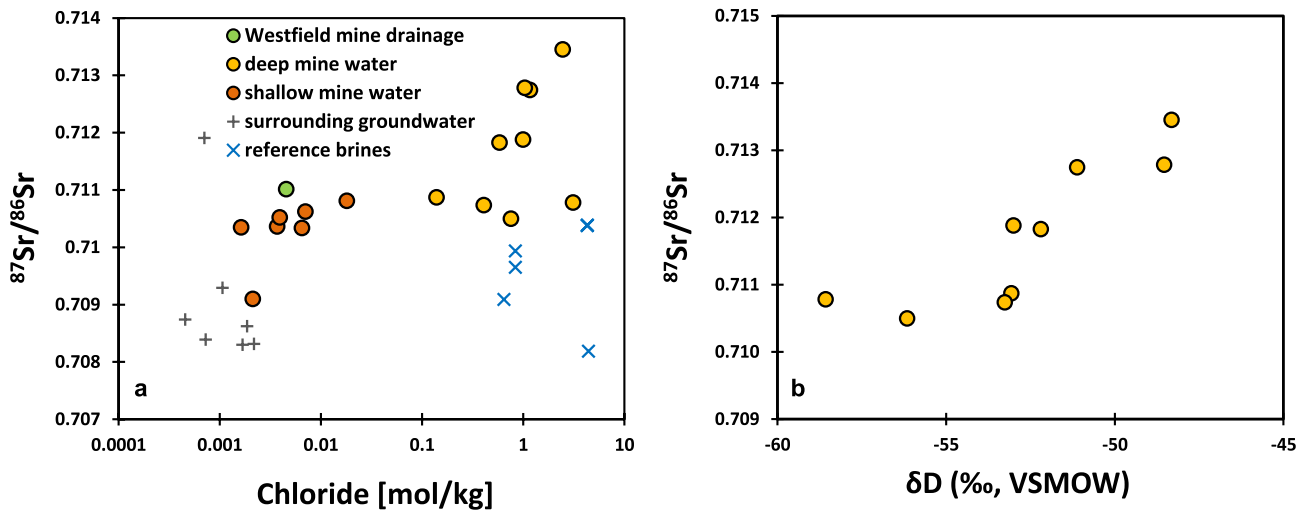


Fig. 10. $^{87}\text{Sr}/^{86}\text{Sr}$ isotope ratio versus chloride [mol/kg] (a), and $^{87}\text{Sr}/^{86}\text{Sr}$ ratio versus δD (‰, VSMOW) (b) in the deep mine water. The correlation indicates a contribution of isotopically heavy connate water to the mine water chemistry.

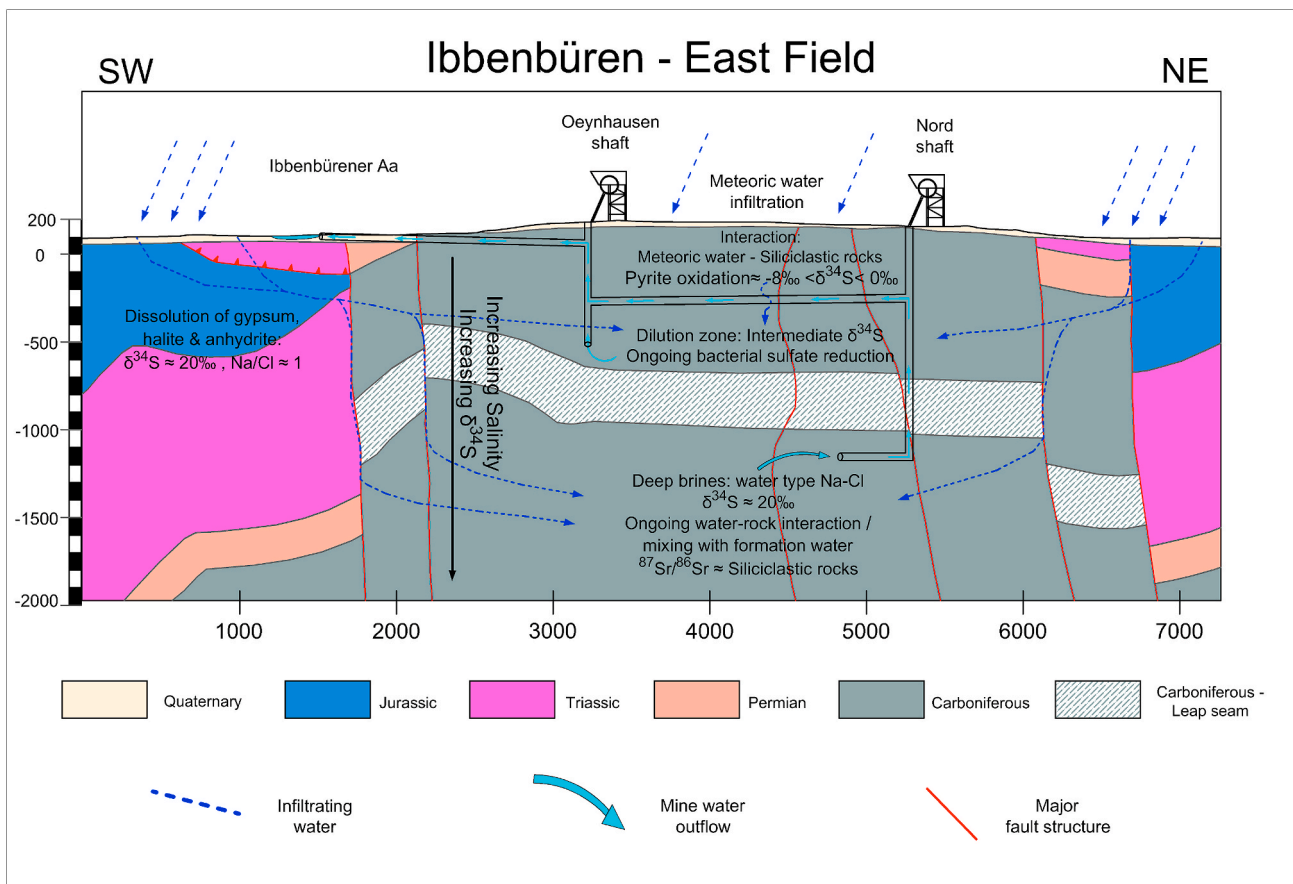


Fig. 11. Schematic cross section through the Ibbenbüren Eastfield including a conceptual hydrogeochemical model, depicting the origin and evolution of mine drainage, groundwater, and brines in the mine. Modified after Drozdowski (1985).

IBB 2 and IBB 3. However, the isotopic composition of fertilizers has also been reported in the same area (Otero et al., 2008).

4.3.4. Strontium isotopes

The $^{87}\text{Sr}/^{86}\text{Sr}$ ratio of the mine waters (IBB-W 1; IBB-E 1 to IBB-E 16) ranges from 0.7091 to 0.7135 (see Table S1 (Supplementary Material) and Fig. 10a). While most of the mine waters plot around $^{87}\text{Sr}/^{86}\text{Sr}$ ratios

from 0.710 to 0.711, the NaCl type brines show a trend towards more radiogenic values with the highest $^{87}\text{Sr}/^{86}\text{Sr}$ ratios of 0.7135 reached in those waters, sampled from the deepest level of the mine. A similar trend has been reported, for instance, by Egeberg and Agaard (1989) for groundwater samples in the North Sea, and by Grobe and Machel (2002) for groundwater from the Münsterland Cretaceous basin. The highly mineralized reference waters have $^{87}\text{Sr}/^{86}\text{Sr}$ ratios between 0.7082 and

0.7104. Compared to the deep mine waters, these Sr isotopic compositions are closer to the range of marine carbonates, likely due to the dissolution of marine evaporites. Nonetheless, with the exception of sample BE 1, taken from a well in the north German basin, the reference brines are isotopically heavy compared to the isotopic signature of the relevant Mesozoic marine evaporites of the region (Burke et al., 1982). The shallow groundwaters (SGW 1 to SGW 6) plot around a $^{87}\text{Sr}/^{86}\text{Sr}$ ratio of 0.709, with the exception SGW 3 that exhibits a value of 0.712.

There is no correlation between strontium content and isotopic signature in the deep mine waters. Normally, the contribution of Sr^{2+} from evaporite dissolution should dominate the isotopic composition (Faure, 2001). Yet, at the Ibbenbüren mine, Sr correlates with alkaline elements. For this reason, the contribution of radiogenic ^{87}Rb from the weathering of Rb-rich minerals such as K-feldspar or muscovite has to be considered in our case, as suggested by Grobe and Machel (2002). The Rb-rich minerals within the Paleozoic rocks might have generated relevant levels of isotopically heavy Sr. Note that a correlation of an increasing $^{87}\text{Sr}/^{86}\text{Sr}$ ratio with increasing $\delta\text{D}_{\text{H}_2\text{O}}$ and $\delta^{18}\text{O}_{\text{H}_2\text{O}}$ values (Fig. 10b) suggests the presence of formation water contributing to the isotopic composition. This is in accordance with the relatively high K^+ and Li^+ concentrations (see above), which cannot be explained by water-rock-interaction at ambient temperature. Formation water, resulting from hydrothermal water-rock interaction, would have reached the necessary temperature.

5. Conclusions

A multi proxy approach including chemical and isotopic analyses was successfully used to elucidate the chemical evolution of mine drainage and groundwater from the Ibbenbüren coal mine (see Fig. 11).

The waters are a result of water-rock interaction, migration, and mixing of different fluids. Mine drainage and groundwater throughout the whole mine show influence of modern meteoric water through δD , $\delta^{18}\text{O}$, and Tritium values. Salinity and sulfur isotopic ratios generally increase with depth.

- (1) Salinity in the deep Na-Cl brines can be assigned to halite dissolution through Na/Cl and Br/Cl ratios. Within the context of the local geological situation, the origin of these brines from outside of the coalfield is corroborated by $\delta^{34}\text{S}_{\text{SO}_4}$ values typical for the dissolution of Mesozoic evaporites that surround the coalfield.
- (2) The mixing of those brines with formation water from the siliclastic rocks of the Carboniferous host rock and ongoing water-rock interaction are indicated by radiogenic strontium, K^+ and Li^+ . The enrichment in alkalis with salinity cannot be attributed to halite dissolution and therefore could result from interaction with the siliclastic rocks of the coalfield. Additionally, a positive correlation of $^{87}\text{Sr}/^{86}\text{Sr}$ with $\delta^2\text{H}_{\text{H}_2\text{O}}$ and $\delta^{18}\text{O}_{\text{H}_2\text{O}}$ values of the mine fluids suggests the presence of formation water, contributing to the water chemistry.
- (3) Shallow mine waters down to the third level ≈ -270 m below surface show a $\delta^{34}\text{S}_{\text{SO}_4}$ composition typical for the oxidation of sulfides. No influence of halite, gypsum, or anhydrite dissolution can be deduced in the shallow waters.
- (4) Intermediate water compositions are a result of mixing between the Na-Cl brines and shallow mine waters. From the co-evolution of $\delta^{34}\text{S}_{\text{SO}_4}$ values and dissolved sulfate together with salinity, only minor influence of bacterial sulfate reduction is suggested in those intermediate waters.

Declaration of competing interest

The authors declare that they have no known competing financial interests or personal relationships that could have appeared to influence the work reported in this paper.

Acknowledgements

This study was funded by Forum Bergbau Wasser. We greatly thank Johannes Wulfert, Heinz Dieter Pollmann, Norbert Schriever, Kai Oppermann, Thomas Heeger, and everybody from RAG Anthrazit Ibbenbüren for facilitating sampling and providing important insights into mine details. We thank Stefanie Eichinger, Judith Jernej and Andrea Wolf at NAWI Graz Central Lab for Water, Minerals and Rocks for the analyses. Thorsten Krämer from Fachklinik Bad Bentheim, Axel Pfeiffer from the city of Bad Rothenfelde, Jules Vleugels from Förderverein Saline Gottesgabe are thanked for allowing us to take samples from the respective brines. We also thank the two anonymous reviewers for their comments and suggestions that helped improve this manuscript.

Appendix A. Supplementary data

Supplementary data to this article can be found online at <https://doi.org/10.1016/j.apgeochem.2020.104693>.

References

- Alcalá, F.J., Custodio, E., 2008. Using the Cl/Br ratio as a tracer to identify the origin of salinity in aquifers in Spain and Portugal. *J. Hydrol.* 359, 189–207. <https://doi.org/10.1016/j.jhydrol.2008.06.028>.
- Antler, G., Turczyn, A.V., Rennie, V., Herut, B., Sivan, O., 2013. Coupled sulfur and oxygen isotope insight into bacterial sulfate reduction in the natural environment. *Geochem. Cosmochim. Acta* 118, 98–117. <https://doi.org/10.1016/j.gca.2013.05.005>.
- Appelo, C.A.J., Postma, D., 2005. *Geochemistry, Groundwater and Pollution*. Balkema.
- Balci, N., Shanks, W.C., Mayer, B., Mandernack, K.W., 2007. Oxygen and sulfur isotope systematics of sulfate produced by bacterial and abiotic oxidation of pyrite. *Geochem. Cosmochim. Acta* 71, 3796–3811. <https://doi.org/10.1016/j.gca.2007.04.017>.
- Banks, D., Burke, S.P., Gray, C.G., 1997. Hydrogeochemistry of coal mine drainage and other ferruginous waters in north Derbyshire and south Yorkshire, UK. *Q. J. Eng. Geol. Hydrogeol.* 30, 257–280. <https://doi.org/10.1144/GSL.QJEG.1997.030.P3.07>.
- Bässler, R., 1970. Hydrogeologische, chemische und Isotopen-Untersuchungen der Grubenwässer des Ibbenbürener Steinkohlenreviers. *Z. Dtsch. Geol. Ges.* 209–286.
- Becker, I., Wüstefeld, P., Koehrer, B., Felder, M., Hilgers, C., 2017. Porosity and permeability variations in a tight gas sandstone reservoir analogue, Westphalian D, Lower Saxony basin, NW Germany: influence of depositional setting and diagenesis. *J. Petrol. Geol.* 40, 363–389. <https://doi.org/10.1111/jpg.12685>.
- Bernardez, L.A., de Andrade Lima, L.R.P., de Jesus, E.B., Ramos, C.L.S., Almeida, P.F., 2013. A kinetic study on bacterial sulfate reduction. *Bioproc. Biosyst. Eng.* 36, 1861–1869. <https://doi.org/10.1007/s00449-013-0960-0>.
- Bernasconi, S.M., Meier, I., Wohlwend, S., Brack, P., Hochuli, P.A., Bläsi, H., Wortmann, U.G., Ramseyer, K., 2017. An evaporite-based high-resolution sulfur isotope record of Late Permian and Triassic seawater sulfate. *Geochem. Cosmochim. Acta* 204, 331–349. <https://doi.org/10.1016/j.gca.2017.01.047>.
- Bibi, I., Singh, B., Silvester, E., 2011. Dissolution of illite in saline-acidic solutions at 25 °C. *Geochem. Cosmochim. Acta* 75, 3237–3249. <https://doi.org/10.1016/j.gca.2011.03.022>.
- Böttcher, J., Strebel, O., Voerkelius, S., Schmidt, H.L., 1990. Using isotope fractionation of nitrate-nitrogen and nitrate-oxygen for evaluation of microbial denitrification in a sandy aquifer. *J. Hydrol.* 114, 413–424. [https://doi.org/10.1016/0022-1694\(90\)90068-9](https://doi.org/10.1016/0022-1694(90)90068-9).
- Böttcher, M.E., Thamdrup, B., Vennemann, T.W., 2001. Oxygen and sulfur isotope fractionation during anaerobic bacterial disproportionation of elemental sulfur. *Geochem. Cosmochim. Acta* 65, 1601–1609. [https://doi.org/10.1016/S0016-7037\(00\)00628-1](https://doi.org/10.1016/S0016-7037(00)00628-1).
- Bottrell, S., Tellam, J., Bartlett, R., Hughes, A., 2008. Isotopic composition of sulfate as a tracer of natural and anthropogenic influences on groundwater geochemistry in an urban sandstone aquifer, Birmingham, UK. *Appl. Geochem.* 23, 2382–2394. <https://doi.org/10.1016/j.apgeochem.2008.03.012>.
- Braitsch, O., Herrmann, A.G., 1963. Zur Geochemie des Broms in salinaren Sedimenten: Teil I: experimentelle Bestimmung der Br-Verteilung in verschiedenen natürlichen Salzsystemen. *Geochem. Cosmochim. Acta* 27, 361–391. [https://doi.org/10.1016/0016-7037\(63\)90077-2](https://doi.org/10.1016/0016-7037(63)90077-2).
- Brand, W.A., Geilmann, H., Crosson, E.R., Rella, C.W., 2009. Cavity ring-down spectroscopy versus high-temperature conversion isotope ratio mass spectrometry; a case study on $\delta^2\text{H}$ and $\delta^{18}\text{O}$ of pure water samples and. *Rapid Commun. Mass Spectrom.* <https://doi.org/10.1002/rcm.4083>.
- Brenot, A., Carignan, J., France-Lanord, C., Benoit, M., 2007. Geological and land use control on $\delta^{34}\text{S}$ and $\delta^{18}\text{O}$ of river dissolved sulfate: the Moselle river basin, France. *Chem. Geol.* 244, 25–41. <https://doi.org/10.1016/j.chemgeo.2007.06.003>.
- Brenot, A., Négrel, P., Petelet-Giraud, E., Millot, R., Malcuit, E., 2015. Insights from the salinity origins and interconnections of aquifers in a regional scale sedimentary aquifer system (Adour-Garonne district, SW France): contributions of $\delta^{34}\text{S}$ and $\delta^{18}\text{O}$

- from dissolved sulfates and the $^{87}\text{Sr}/^{86}\text{Sr}$ ratio. *Appl. Geochem.* 53, 27–41. <https://doi.org/10.1016/J.APGEOCHEM.2014.12.002>.
- Brunner, B., Bernasconi, S.M., Kleikemper, J., Schroth, M.H., 2005. A model for oxygen and sulfur isotope fractionation in sulfate during bacterial sulfate reduction processes. *Geochem. Cosmochim. Acta* 69, 4773–4785. <https://doi.org/10.1016/J.GCA.2005.04.017>.
- Bruns, B., di Primio, R., Berner, U., Littke, R., 2013. Petroleum system evolution in the inverted Lower Saxony Basin, northwest Germany: a 3D basin modeling study. *Geofluids* 13, 246–271. <https://doi.org/10.1111/gf.12016>.
- Bruns, B., Littke, R., 2015. Lithological dependency and anisotropy of vitrinite reflectance in high rank sedimentary rocks of the Ibbenbüren area, NW-Germany: implications for the tectonic and thermal evolution of the Lower Saxony Basin. *Int. J. Coal Geol.* 137, 124–135. <https://doi.org/10.1016/J.COAL.2014.11.007>.
- Burke, A., Present, T.M., Paris, G., Rae, E.C.M., Sandilands, B.H., Gaillardet, J., Peucker-Ehrenbrink, B., Fischer, W.W., McClelland, J.W., Spencer, R.G.M., Voss, B.M., Adkins, J.F., 2018. Sulfur isotopes in rivers: insights into global weathering budgets, pyrite oxidation, and the modern sulfur cycle. *Earth Planet Sci. Lett.* 496, 168–177. <https://doi.org/10.1016/J.EPSL.2018.05.022>.
- Burke, W.H., Denison, R.E., Hetherington, E.A., Koepnick, R.B., Nelson, H.F., Otto, J.B., 1982. Variation of seawater $^{87}\text{Sr}/^{86}\text{Sr}$ throughout Phanerozoic time. *Geology* 10 (516). [https://doi.org/10.1130/0091-7613\(1982\)10<516:VOSSTP>2.0.CO;2](https://doi.org/10.1130/0091-7613(1982)10<516:VOSSTP>2.0.CO;2).
- Cañedo-Argüelles, M., Kefford, B.J., Piscart, C., Prat, N., Schäfer, R.B., Schulz, C.-J., 2013. Salinisation of rivers: an urgent ecological issue. *Environ. Pollut.* 173, 157–167. <https://doi.org/10.1016/J.ENVPOL.2012.10.011>.
- Chan, L.-H., Starinsky, A., Katz, A., 2002. The behavior of lithium and its isotopes in oilfield brines: evidence from the Heletz-Kokhav field, Israel. *Geochem. Cosmochim. Acta* 66, 615–623. [https://doi.org/10.1016/S0016-7037\(01\)00800-6](https://doi.org/10.1016/S0016-7037(01)00800-6).
- Chowdhury, A.H., Scanlon, B.R., Reedy, R.C., Young, S., 2018. Fingerprinting groundwater salinity sources in the gulf coast aquifer system, USA. *Hydrogeol. J.* 26, 197–213. <https://doi.org/10.1007/s10040-017-1619-8>.
- Claypool, G.E., Holser, W.T., Kaplan, I.R., Sakai, H., Zak, I., 1980. The age curves of sulfur and oxygen isotopes in marine sulfate and their mutual interpretation. *Chem. Geol.* 28, 199–260. [https://doi.org/10.1016/0009-2541\(80\)90047-9](https://doi.org/10.1016/0009-2541(80)90047-9).
- Craig, H., 1961. Isotopic variations in meteoric waters. *Science* 133, 1702–1703. <https://doi.org/10.1126/science.133.3465.1702>.
- Cravotta, C.A., Brady, K.B.C., 2015. Priority pollutants and associated constituents in untreated and treated discharges from coal mining or processing facilities in Pennsylvania, USA. *Appl. Geochem.* 62, 108–130. <https://doi.org/10.1016/J.APGEOCHEM.2015.03.001>.
- Davis, S.N., Whittemore, D.O., Fabryka-Martin, J., 1998. Uses of chloride/bromide ratios in studies of potable water. *Ground Water* 36, 338–350. <https://doi.org/10.1111/j.1745-6584.1998.tb01099.x>.
- Dogramaci, S.S., Herczeg, A.L., Schiff, S.L., Bone, Y., 2001. Controls on $\delta^{34}\text{S}$ and $\delta^{18}\text{O}$ of dissolved sulfate in aquifers of the murray basin, Australia and their use as indicators of flow processes. *Appl. Geochem.* 16, 475–488. [https://doi.org/10.1016/S0883-2927\(00\)0052-4](https://doi.org/10.1016/S0883-2927(00)0052-4).
- Dold, B., 2017. Acid rock drainage prediction: a critical review. *J. Geochem. Explor.* 172, 120–132. <https://doi.org/10.1016/J.GEXPLO.2016.09.014>.
- Dölling, M., Strizke, R., 2009. Geowissenschaftliche Untersuchungen im Subrosionsgebiet des „Heiligen Feldes“ (nördliches Münsterland, Nordwestdeutschland). *Geol. Palaontol. Westfalen* 72, 31–69.
- Drake, H., Whitehouse, M.J., Heim, C., Reiners, P.W., Tillberg, M., Hogmalm, K.J., Dopson, M., Broman, C., Åström, M.E., 2018. Unprecedented ^{34}S -enrichment of pyrite formed following microbial sulfate reduction in fractured crystalline rocks. *Geobiology* 16, 556–574. <https://doi.org/10.1111/gbi.12297>.
- Drozdowski, G., 1985. Tiefentektonik der Ibbenbürener Karbonscholle. In: *Beiträge Zur Tiefentektonik Westdeutscher Steinkohlelagerstätten. Geologisches Landesamt Nordrhein-Westfalen*, pp. 189–216.
- Egeberg, P.K., Aagaard, P., 1989. Origin and evolution of formation waters from oil fields on the Norwegian shelf. *Appl. Geochem.* 4, 131–142. [https://doi.org/10.1016/0883-2927\(89\)90044-9](https://doi.org/10.1016/0883-2927(89)90044-9).
- Ehrenberg, S.N., 1991. Kaolinized, potassium-leached zones at the contacts of the Garn Formation, Haltenbanken, mid-Norwegian continental shelf. *Mar. Petrol. Geol.* 8, 250–269. [https://doi.org/10.1016/0264-8172\(91\)90080-K](https://doi.org/10.1016/0264-8172(91)90080-K).
- Elphick, J.R.F., Bergh, K.D., Bailey, H.C., 2011. Chronic toxicity of chloride to freshwater species: effects of hardness and implications for water quality guidelines. *Environ. Toxicol. Chem.* 30, 239–246. <https://doi.org/10.1002/etc.365>.
- Epstein, S., Mayeda, T., 1953. Variation of O^{18} content of waters from natural sources. *Geochem. Cosmochim. Acta* 4, 213–224. [https://doi.org/10.1016/0016-7037\(53\)90051-9](https://doi.org/10.1016/0016-7037(53)90051-9).
- Faure, G., 2001. *Origin of Igneous Rocks, Origin of Igneous Rocks*. Springer Berlin Heidelberg. <https://doi.org/10.1007/978-3-662-04474-2>.
- Fontes, J.C., Matray, J.M., 1993a. Geochemistry and origin of formation brines from the Paris Basin, France: 1. Brines associated with Triassic salts. *Chem. Geol.* 109, 149–175. [https://doi.org/10.1016/0009-2541\(93\)90068-T](https://doi.org/10.1016/0009-2541(93)90068-T).
- Fontes, J.C., Matray, J.M., 1993b. Geochemistry and origin of formation brines from the Paris Basin, France: 2. Saline solutions associated with oil fields. *Chem. Geol.* 109, 177–200. [https://doi.org/10.1016/0009-2541\(93\)90069-U](https://doi.org/10.1016/0009-2541(93)90069-U).
- Foriel, J., Philippot, P., Rey, P., Somogyi, A., Banks, D., Ménez, B., 2004. Biological control of Cl/Br and low sulfate concentration in a 3.5-Gyr-old seawater from North Pole, Western Australia. *Earth Planet Sci. Lett.* 228, 451–463. <https://doi.org/10.1016/J.EPSL.2004.09.034>.
- Foti, M., Sorokin, D.Y., Lomans, B., Mussman, M., Zacharova, E.E., Pimenov, N.V., Kuenen, J.G., Muyzer, G., 2007. Diversity, activity, and abundance of sulfate-reducing bacteria in saline and hypersaline soda lakes. *Appl. Environ. Microbiol.* 73, 2093–2100. <https://doi.org/10.1128/AEM.02622-06>.
- Fritz, P., Basharmal, G.M., Drimmie, R.J., Ibsen, J., Qureshi, R.M., 1989. Oxygen isotope exchange between sulphate and water during bacterial reduction of sulphate. *Chem. Geol. Isot. Geosci.* 79, 99–105. [https://doi.org/10.1016/0168-9622\(89\)90012-2](https://doi.org/10.1016/0168-9622(89)90012-2).
- Galán, E., Gómez-Ariza, J., González, I., Fernández-Caliani, J., Morales, E., Giráldez, I., 2003. Heavy metal partitioning in river sediments severely polluted by acid mine drainage in the Iberian Pyrite Belt. *Appl. Geochem.* 18, 409–421. [https://doi.org/10.1016/S0883-2927\(02\)00092-6](https://doi.org/10.1016/S0883-2927(02)00092-6).
- Gammons, C.H., Brown, A., Poulson, S.R., Henderson, T.H., 2013. Using stable isotopes (S, O) of sulfate to track local contamination of the Madison karst aquifer, Montana, from abandoned coal mine drainage. *Appl. Geochem.* 31, 228–238. <https://doi.org/10.1016/J.APGEOCHEM.2013.01.008>.
- Gazea, B., Adam, K., Kontopoulos, A., 1996. A review of passive systems for the treatment of acid mine drainage. *Miner. Eng.* 9, 23–42. [https://doi.org/10.1016/0892-6875\(95\)00129-8](https://doi.org/10.1016/0892-6875(95)00129-8).
- Gombert, P., Sracek, O., Koukouzas, N., Gzyl, G., Valladares, S.T., Frączek, R., Klinger, C., Bauerek, A., Areces, J.E.A., Chamberlain, S., Paw, K., Pierzchała, L., 2018. An overview of priority pollutants in selected coal mine discharges in Europe. *Mine Water Environ.* 1–8. <https://doi.org/10.1007/s10230-018-0547-8>.
- Grobe, M., Machel, H.G., 2002. Saline groundwater in the Münsterland Cretaceous Basin, Germany: clues to its origin and evolution. *Mar. Petrol. Geol.* 19, 307–322. [https://doi.org/10.1016/S0264-8172\(02\)00019-3](https://doi.org/10.1016/S0264-8172(02)00019-3).
- Habicht, K.S., Canfield, D.E., 1997. Sulfur isotope fractionation during bacterial sulfate reduction in organic-rich sediments. *Geochem. Cosmochim. Acta* 61, 5351–5361. [https://doi.org/10.1016/S0016-7037\(97\)00311-6](https://doi.org/10.1016/S0016-7037(97)00311-6).
- Hardie, L., Eugster, H., 1971. Evaporation of seawater: calculated mineral sequences. *Science* 173, 481–489. <https://doi.org/10.1126/science.173.3996.481>.
- Hart, B.T., Bailey, P., Edwards, R., Hortle, K., James, K., McMahon, A., Meredith, C., Swadling, K., 1991. A review of the salt sensitivity of the Australian freshwater biota. *Hydrobiologia* 210, 105–144. <https://doi.org/10.1007/BF00014327>.
- Haubrich, F., Tichomirowa, M., 2002. Sulfur and oxygen isotope geochemistry of acid mine drainage—the polymetallic sulfide deposit “Himmelfahrt Fundgrube” in Freiberg (Germany). *Isot. Environ. Health Stud.* 38, 121–138. <https://doi.org/10.1080/10256010208033319>.
- Hayes, J.M., 2004. *An Introduction to Isotopic Calculations*. Woods Hole Oceanographic Institution, Woods Hole, MA, p. 2543.
- Heidel, C., Tichomirowa, M., 2011. The isotopic composition of sulfate from anaerobic and low oxygen pyrite oxidation experiments with ferric iron - new insights into oxidation mechanisms. *Chem. Geol.* 281, 305–316. <https://doi.org/10.1016/j.chemgeo.2010.12.017>.
- Heidel, C., Tichomirowa, M., Breitkopf, C., 2011. Sphalerite oxidation pathways detected by oxygen and sulfur isotope studies. *Appl. Geochem.* 26, 2247–2259. <https://doi.org/10.1016/j.apgeochem.2011.08.007>.
- Heidel, C., Tichomirowa, M., Junghans, M., 2013. Oxygen and sulfur isotope investigations of the oxidation of sulfide mixtures containing pyrite, Galena, and sphalerite. *Chem. Geol.* 342, 29–43. <https://doi.org/10.1016/j.chemgeo.2013.01.016>.
- Holser, W.T., Kaplan, I.R., 1966. Isotope geochemistry of sedimentary sulfates. *Chem. Geol.* 1, 93–135. [https://doi.org/10.1016/0009-2541\(66\)90011-8](https://doi.org/10.1016/0009-2541(66)90011-8).
- Horita, J., 1988. Hydrogen isotope analysis of natural waters using an H_2 -water equilibration method: a special implication to brines. *Chem. Geol. Isot. Geosci.* 72, 89–94. [https://doi.org/10.1016/0168-9622\(88\)90040-1](https://doi.org/10.1016/0168-9622(88)90040-1).
- Horita, J., Friedman, T.J., Lazar, B., Holland, H.D., 1991. The composition of Permian seawater. *Geochem. Cosmochim. Acta* 55, 417–432. [https://doi.org/10.1016/0016-7037\(91\)90001-L](https://doi.org/10.1016/0016-7037(91)90001-L).
- Horita, J., Ueda, A., Mizukami, K., Takatori, I., 1989. Automatic δD and $\delta^{18}\text{O}$ analyses of multi-water samples using H_2 - and CO_2 -water equilibration methods with a common equilibration set-up. *Int. J. Radiat. Appl. Instrum. Part 40*, 801–805. [https://doi.org/10.1016/0883-2889\(89\)90100-7](https://doi.org/10.1016/0883-2889(89)90100-7).
- Horita, J., Zimmermann, H., Holland, H.D., 2002. Chemical evolution of seawater during the Phanerozoic: implications from the record of marine evaporites. *Geochem. Cosmochim. Acta* 66, 3733–3756. [https://doi.org/10.1016/S0016-7037\(01\)00884-5](https://doi.org/10.1016/S0016-7037(01)00884-5).
- Johnson, D.B., Hallberg, K.B., 2005. Acid mine drainage remediation options: a review. *Sci. Total Environ.* 338, 3–14. <https://doi.org/10.1016/J.SCITOTENV.2004.09.002>.
- Kampschulte, A., Strauss, H., 2004. The sulfur isotopic evolution of Phanerozoic seawater based on the analysis of structurally substituted sulfate in carbonates. *Chem. Geol.* 204, 255–286. <https://doi.org/10.1016/J.CHEMGEO.2003.11.013>.
- Katz, B.G., Eberts, S.M., Kauffman, L.J., 2011. Using Cl/Br ratios and other indicators to assess potential impacts on groundwater quality from septic systems: a review and examples from principal aquifers in the United States. *J. Hydrol.* 397, 151–166. <https://doi.org/10.1016/J.JHYDROL.2010.11.017>.
- Kendall, C., Doctor, D.H., 2003. Stable isotope applications in hydrologic studies. In: *Treatise on Geochemistry*, pp. 319–364. <https://doi.org/10.1016/B0-08-043751-6/05081-7>.
- Kloppmann, W., Négrel, P., Casanova, J., Klinge, H., Schelkes, K., Guerrot, C., 2001. Halite dissolution derived brines in the vicinity of a Permian salt dome (N German Basin). Evidence from boron, strontium, oxygen, and hydrogen isotopes. *Geochem. Cosmochim. Acta* 65, 4087–4101. [https://doi.org/10.1016/S0016-7037\(01\)00640-8](https://doi.org/10.1016/S0016-7037(01)00640-8).
- Knauth, L.P., Beeunas, M.A., 1986. Isotope geochemistry of fluid inclusions in Permian halite with implications for the isotopic history of ocean water and the origin of saline formation waters. *Geochem. Cosmochim. Acta* 50, 419–433. [https://doi.org/10.1016/0016-7037\(86\)90195-X](https://doi.org/10.1016/0016-7037(86)90195-X).
- Knöller, K., Fauville, A., Mayer, B., Strauch, G., Friese, K., Veizer, J., 2004. Sulfur cycling in an acid mining lake and its vicinity in Lusatia, Germany. *Chem. Geol.* 204, 303–323. <https://doi.org/10.1016/J.CHEMGEO.2003.11.009>.

- Lotze, F., Semmler, W., Kötter, K., Mausolf, F., 1962. Hydrogeologie des Westteils der Ibbenbürener Karbonscholle. Springer Fachmedien Wiesbaden GmbH. <https://doi.org/10.1007/978-3-6663-02578-8>.
- MacCausland, A., McTammany, M.E., 2007. The impact of episodic coal mine drainage pollution on benthic macroinvertebrates in streams in the Anthracite region of Pennsylvania. *Environ. Pollut.* 149, 216–226. <https://doi.org/10.1016/j.envpol.2006.12.030>.
- McCaffrey, M.A., Lazar, B., Holland, H.D., 1987. The evaporation path of seawater and the coprecipitation of Br⁻ and K⁺ with halite. *J. Sediment. Petrol.* 57, 928–938.
- McKnight, D.M., Feder, G.L., 1984. The ecological effect of acid conditions and precipitation of hydrous metal oxides in a Rocky Mountain stream. *Hydrobiologia* 119, 129–138. <https://doi.org/10.1007/BF00011952>.
- Migaszweski, Z.M., Gaiuska, A., Dołęgowska, S., 2018. Stable isotope geochemistry of acid mine drainage from the Wiśniówka area (south-central Poland). *Appl. Geochem.* 95, 45–56. <https://doi.org/10.1016/j.apgeochem.2018.05.015>.
- Millero, F.J., Feistel, R., Wright, D.G., McDougall, T.J., 2008. The composition of standard seawater and the definition of the reference-composition salinity scale. *Deep-Sea Res. Part I Oceanogr. Res. Pap.* 55, 50–72. <https://doi.org/10.1016/j.dsr.2007.10.001>.
- MKULMV, 2016. Hintergrundpapier Steinkohle zum Bewirtschaftungsplan 2019-2021 für die nordrhein-westfälischen Anteile von Rhein, Weser, Ems und Maas. *Arnsberg*.
- Moodley, I., Sheridan, C.M., Kappelmeyer, U., Akcil, A., 2018. Environmentally sustainable acid mine drainage remediation: research developments with a focus on waste/by-products. *Miner. Eng.* 126, 207–220. <https://doi.org/10.1016/j.mineng.2017.08.008>.
- Müller, G., Nielsen, H., Ricke, W., 1966. Schwefel-Isotopen-Verhältnisse in Formationswässern und Evaporiten Nord- und Süddeutschlands. *Chem. Geol.* 1, 211–220. [https://doi.org/10.1016/0009-2541\(66\)90017-9](https://doi.org/10.1016/0009-2541(66)90017-9).
- Munoz, Y.A., Littke, R., Brix, M.R., 2007. Fluid systems and basin evolution of the western Lower Saxony Basin, Germany. *Geofluids* 7, 335–355. <https://doi.org/10.1111/j.1468-8123.2007.00186.x>.
- Naidu, G., Ryu, S., Thiruvengatachari, R., Choi, Y., Jeong, S., Vigneswaran, S., 2019. A critical review on remediation, reuse, and resource recovery from acid mine drainage. *Environ. Pollut.* 247, 1110–1124. <https://doi.org/10.1016/j.envpol.2019.01.085>.
- Neal, C., Whitehead, P.G., Jeffery, H., Neal, M., 2005. The water quality of the river Carnon, west Cornwall, November 1992 to March 1994: the impacts of wheal Jane discharges. *Sci. Total Environ.* 338, 23–39. <https://doi.org/10.1016/j.scitotenv.2004.09.003>.
- Nieto, J.M., Sarmiento, A.M., Ollás, M., Canovas, C.R., Riba, I., Kalman, J., Delvals, T.A., 2007. Acid mine drainage pollution in the Tinto and Odiel rivers (Iberian pyrite belt, SW Spain) and bioavailability of the transported metals to the Huelva estuary. *Environ. Int.* 33, 445–455. <https://doi.org/10.1016/j.envint.2006.11.010>.
- Novák, M., Jäcková, I., Prechová, E., 2001. Temporal trends in the isotope signature of air-borne sulfur in Central Europe. *Environ. Sci. Technol.* 35, 255–260. <https://doi.org/10.1021/es0000753>.
- Oren, A., 1999. Bioenergetic aspects of halophilism. *Microbiol. Mol. Biol. Rev.* 63, 334–348. <https://doi.org/10.1128/mmb.63.2.334-348.1999>.
- Otero, N., Soler, A., 2002. Sulphur isotopes as tracers of the influence of potash mining in groundwater salinisation in the Llobregat Basin (NE Spain). *Water Res.* 36, 3989–4000. [https://doi.org/10.1016/S0043-1354\(02\)00125-2](https://doi.org/10.1016/S0043-1354(02)00125-2).
- Otero, N., Soler, A., Canals, A., 2008. Controls of $\delta^{34}\text{S}$ and $\delta^{18}\text{O}$ in dissolved sulphate: learning from a detailed survey in the Llobregat River (Spain). *Appl. Geochem.* 23, 1166–1185. <https://doi.org/10.1016/j.apgeochem.2007.11.009>.
- Panno, S.V., Hackley, K.C., Hwang, H.H., Greenberg, S.E., Krapac, I.G., Landsberger, S., O'Kelly, D.J., 2006. Characterization and identification of Na-Cl sources in ground water. *Ground Water* 44, 176–187. <https://doi.org/10.1111/j.1745-6584.2005.00127.x>.
- Parbhakar-Fox, A., Lottermoser, B.G., 2015. A critical review of acid rock drainage prediction methods and practices. *Miner. Eng.* 82, 107–124. <https://doi.org/10.1016/j.mineng.2015.03.015>.
- Parkhurst, D.L., Appelo, C.A.J., 1999. User's Guide to PHREEQC (Version 2) : a Computer Program for Speciation, Batch-Reaction, One-Dimensional Transport, and Inverse Geochemical Calculations, Water-Resources Investigations Report. <https://doi.org/10.3133/wri994259>.
- Pfahl, S., Sodemann, H., 2014. What controls deuterium excess in global precipitation? *Clim. Past* 10, 771–781. <https://doi.org/10.5194/cp-10-771-2014>.
- Révész, K., Haiping, Q., Coplen, T.B., 2012. Determination of the $\delta^{34}\text{S}$ of sulfate in water; *RSIL lab code 1951*, chap. 10 of Stable isotope-ratio methods, sec. C. In: *Book 10, Methods of the Reston Stable Isotope Laboratory*.
- Riley, J.P., Tongudai, M., 1964. The lithium content of sea water. *Deep Sea Res. Oceanogr. Abstr.* 11, 563–568. [https://doi.org/10.1016/0011-7471\(64\)90002-6](https://doi.org/10.1016/0011-7471(64)90002-6).
- Rudakov, Dmitry V., Coldewey, Wilhelm G., Goerke-Mallet, P., 2014. Modeling the inflow and discharge from underground structures within the abandoned hardcoal mining area of west field (Ibbenbüren). In: Sui, Wanghua, Sun, Yajun, Wang, C. (Eds.), *An Interdisciplinary Response to Mine Water Challenges. 12th International Mine Water Association Congress (IMWA 2014)*. China University of Mining and Technology, Xuzhou, China, pp. 699–705.
- Schlosser, P., Stute, M., Dörr, H., Sonntag, C., Münnich, K.O., 1988. Tritium/³He dating of shallow groundwater. *Earth Planet Sci. Lett.* 89, 353–362. [https://doi.org/10.1016/0012-821X\(88\)90122-7](https://doi.org/10.1016/0012-821X(88)90122-7).
- Scott, A.D., Smith, S.J., 1966. Susceptibility of interlayer potassium in micas to exchange with sodium. *Clay Clay Miner.* 69–81. <https://doi.org/10.1016/B978-0-08-011908-3.50008-6>.
- Scullion, J., Edwards, R.W., 1980. The effect of pollutants from the coal industry on the fish fauna of a small river in the South Wales coalfield. *Environ. Pollut. Ecol. Biol.* 21, 141–153. [https://doi.org/10.1016/0143-1471\(80\)90042-2](https://doi.org/10.1016/0143-1471(80)90042-2).
- Seal, R.R., 2006. Sulfur isotope geochemistry of sulfide minerals. *Rev. Mineral. Geochem.* 61, 633–677. <https://doi.org/10.2138/rmg.2006.61.12>.
- Senglaub, Y., Brix, M.R., Adriasola, A.C., Littke, R., 2005. New information on the thermal history of the southwestern Lower Saxony Basin, northern Germany, based on fission track analysis. *Int. J. Earth Sci.* 94, 876–896. <https://doi.org/10.1007/s00531-005-0008-z>.
- Shalev, N., Lazar, B., Köbberich, M., Halicz, L., Gavrieli, I., 2018. The chemical evolution of brine and Mg-K-salts along the course of extreme evaporation of seawater – an experimental study. *Geochem. Cosmochim. Acta* 241, 164–179. <https://doi.org/10.1016/j.gca.2018.09.003>.
- Siemann, M.G., Schramm, M., 2000. Thermodynamic modelling of the Br partition between aqueous solutions and halite. *Geochem. Cosmochim. Acta* 64, 1681–1693. [https://doi.org/10.1016/S0016-7037\(99\)00385-3](https://doi.org/10.1016/S0016-7037(99)00385-3).
- Simate, G.S., Ndlovu, S., 2014. Acid mine drainage: challenges and opportunities. *J. Environ. Chem. Eng.* 2, 1785–1803. <https://doi.org/10.1016/j.jece.2014.07.021>.
- Stammeier, J.A., Hippler, D., Nebel, O., Leis, A., Grengg, C., Mittermayr, F., Kasemann, S.A., Dietzel, M., 2019. Radiogenic Sr and stable C and O isotopes across Precambrian-Cambrian transition in marine carbonatic phosphorites of Malý Karatau (Kazakhstan)—implications for Paleo-environmental change. *G-cubed* 20, 3–23. <https://doi.org/10.1029/2018GC007767>.
- Strauss, H., 1997. The isotopic composition of sedimentary sulfur through time. *Palaeogeogr. Palaeoclimatol. Palaeoecol.* 132, 97–118. [https://doi.org/10.1016/S0031-0182\(97\)00067-9](https://doi.org/10.1016/S0031-0182(97)00067-9).
- Stueber, A.M., Walter, L.M., Huston, T.J., Pushkar, P., 1993. Formation waters from Mississippian-Pennsylvanian reservoirs, Illinois basin, USA: chemical and isotopic constraints on evolution and migration. *Geochem. Cosmochim. Acta* 57, 763–784. [https://doi.org/10.1016/0016-7037\(93\)90167-U](https://doi.org/10.1016/0016-7037(93)90167-U).
- Stumpp, C., Klaus, J., Stichler, W., 2014. Analysis of long-term stable isotopic composition in German precipitation. *J. Hydrol.* 517, 351–361. <https://doi.org/10.1016/j.jhydrol.2014.05.034>.
- Taylor, B.E., Wheeler, M.C., Nordstrom, D.K., 1984. Stable isotope geochemistry of acid mine drainage: experimental oxidation of pyrite. *Geochem. Cosmochim. Acta* 48, 2669–2678. [https://doi.org/10.1016/0016-7037\(84\)90315-6](https://doi.org/10.1016/0016-7037(84)90315-6).
- Thamdrup, B., Finster, K., Hansen, J.W., Bak, F., 1993. Bacterial disproportionation of elemental sulfur coupled to chemical reduction of iron or manganese. *Appl. Environ. Microbiol.* 59, 101–108.
- Thyne, G., Boudreau, B.P., Ramm, M., Midtbø, R.E., 2001. Simulation of potassium feldspar dissolution and illitization in the Staffjord formation, North Sea. *Am. Assoc. Petrol. Geol. Bull.* 85, 621–635. <https://doi.org/10.1306/8626C965-173B-11D7-8645000102C1865D>.
- Tichomirowa, M., Heidel, C., Junghans, M., Haubrich, F., Matschullat, J., 2010. Sulfate and strontium water source identification by O, S and Sr isotopes and their temporal changes (1997–2008) in the region of Freiberg, central-eastern Germany. *Chem. Geol.* 276, 104–118. <https://doi.org/10.1016/j.chemgeo.2010.06.004>.
- Timpano, A.J., Schoenholtz, S.H., Soucek, D.J., Zipper, C.E., 2015. Salinity as a limiting factor for biological condition in mining-influenced central Appalachian headwater streams. *J. Am. Water Resour. Assoc.* 51, 240–250. <https://doi.org/10.1111/jawr.12247>.
- Turchyn, A.V., Schrag, D.P., 2006. Cenozoic evolution of the sulfur cycle: insight from oxygen isotopes in marine sulfate. *Earth Planet Sci. Lett.* 241, 763–779. <https://doi.org/10.1016/j.epsl.2005.11.007>.
- Turek, M., 2004. Electrodialytic desalination and concentration of coal-mine brine. *Desalination* 162, 355–359. [https://doi.org/10.1016/S0011-9164\(04\)00069-4](https://doi.org/10.1016/S0011-9164(04)00069-4).
- Utrilla, R., Pierre, C., Orti, F., Pueyo, J.J., 1992. Oxygen and sulphur isotope compositions as indicators of the origin of Mesozoic and Cenozoic evaporites from Spain. *Chem. Geol.* 102, 229–244. [https://doi.org/10.1016/0009-2541\(92\)90158-2](https://doi.org/10.1016/0009-2541(92)90158-2).
- Wang, N., Dorman, R.A., Ingersoll, C.G., Hardesty, D.K., Brumbaugh, W.G., Hammer, E.J., Bauer, C.R., Mount, D.R., 2016. Acute and chronic toxicity of sodium sulfate to four freshwater organisms in water-only exposures. *Environ. Toxicol. Chem.* 35, 115–127. <https://doi.org/10.1002/etc.3148>.
- Wendland, F., Hannappel, S., Kunkel, R., Schenk, R., Voigt, H.J., Wolter, R., 2005. A procedure to define natural groundwater conditions of groundwater bodies in Germany. *Water Sci. Technol.* 51, 249–257. <https://doi.org/10.2166/wst.2005.0598>.
- Wilkinson, M., Haszeldine, R.S., Morton, A., Fallick, A.E., 2014. Deep burial dissolution of K-feldspars in a fluvial sandstone, Pentland formation, UK central North Sea. *J. Geol. Soc. (Lond.)* 171, 635–647. <https://doi.org/10.1144/jgs2013-144>.
- Wolkersdorfer, C., 2008. Water Management at Abandoned Flooded Underground Mines. Springer, Berlin, Heidelberg. <https://doi.org/10.1007/978-3-540-77331-3>.
- Wüstefeld, P., Hilde, U., Koehler, B., Adelmann, D., Hilgers, C., 2017. Critical evaluation of an Upper Carboniferous tight gas sandstone reservoir analog: diagenesis and petrophysical aspects. *Mar. Petrol. Geol.* 86, 689–710. <https://doi.org/10.1016/j.marpetgeo.2017.05.034>.
- Zhang, Y.C., Slomp, C.P., Broers, H.P., Passier, H.F., Cappellen, P. Van, 2009. Denitrification coupled to pyrite oxidation and changes in groundwater quality in a shallow sandy aquifer. *Geochem. Cosmochim. Acta* 73, 6716–6726. <https://doi.org/10.1016/j.gca.2009.08.026>.
- Zhu, C., 2005. In situ feldspar dissolution rates in an aquifer. *Geochem. Cosmochim. Acta* 69, 1435–1453. <https://doi.org/10.1016/j.gca.2004.09.005>.

Sample	Depth	water type	I	EC ₂₅	pH	Temp	DO	CBE	Density	Na	K	Ca	Mg	Sr
	[m]		[mol/kg]	[μS/cm]		[°C]	[mg/l]	%	[kg/l]	[mol/kg]	[mol/kg]	[mol/kg]	[mol/kg]	[mol/kg]
IBB-W 1	-	Ca-Mg-Na-SO4	0.05	3169	6.3	14	4.3	0.7	1.00	9.78E-03	2.52E-04	6.63E-03	4.92E-03	1.06E-05
IBB-E 1	-1414	Na-Cl	1.03	82568	7.1	27	1.9	-0.6	1.04	9.70E-01	2.91E-03	8.67E-03	5.71E-03	2.30E-04
IBB-E 2	-1482	Na-Cl	1.20	93353	6.6	38	1.9	-0.1	1.04	1.13E+00	2.67E-03	9.56E-03	7.88E-03	2.97E-04
IBB-E 3	-1405	Na-Cl	3.18	187810	6.0	43	0.5	-0.7	1.10	3.02E+00	7.24E-03	2.14E-02	1.48E-02	3.54E-04
IBB-E 4	-1470	Na-Cl	2.53	160520	6.5	32	1.1	-0.9	1.09	2.32E+00	3.31E-03	3.21E-02	2.23E-02	8.94E-04
IBB-E 5	-509	Na-Cl	0.17	15816	7.4	13	4.7	-0.4	1.01	1.35E-01	5.73E-04	6.65E-03	3.93E-03	4.27E-05
IBB-E 6	-716	Na-Cl	0.82	66507	6.7	18	2.2	-0.9	1.03	6.93E-01	2.49E-03	2.92E-02	1.07E-02	2.51E-04
IBB-E 7	-371	Na-Cl	0.46	40111	6.6	12	3.2	-0.3	1.02	3.72E-01	1.46E-03	1.97E-02	7.91E-03	1.33E-04
IBB-E 8	0	Na-Cl	0.62	53647	7.0	16	6.6	-0.3	1.02	5.53E-01	1.49E-03	1.42E-02	6.97E-03	1.73E-04
IBB-E 9	-1208	Na-Cl	1.07	84899	7.1	27	4.3	-0.5	1.04	9.92E-01	2.63E-03	1.17E-02	9.02E-03	2.18E-04
IBB-E 10	-264	Na-Ca-SO4-Cl-HCO3	0.02	1696	7.8	12	8.6	-6.1	1.00	6.98E-03	1.08E-04	3.23E-03	1.27E-03	9.82E-06
IBB-E 11	-123	Ca-SO4-HCO3-Cl	0.01	833	7.2	10	4.7	-2.5	1.00	1.53E-03	1.20E-04	2.37E-03	8.22E-04	3.77E-06
IBB-E 12	-77.3	Ca-Na-SO4-Cl-HCO3	0.01	1073	6.7	9	3.0	-7.1	1.00	3.01E-03	6.42E-05	2.18E-03	9.51E-04	2.51E-06
IBB-E 13	-126	Na-Ca-Cl	0.03	2441	7.0	11	7.9	-2.0	1.00	1.36E-02	1.17E-04	2.51E-03	1.09E-03	5.48E-06
IBB-E 14	-263	Ca-Mg-Na-SO4-Cl	0.03	2286	6.5	9	7.2	0.4	1.00	5.22E-03	1.26E-04	6.13E-03	2.92E-03	6.16E-06
IBB-E 15	-260	Ca-Mg-Na-SO4-Cl	0.03	1625	6.4	9	7.4	-0.2	1.00	3.44E-03	1.24E-04	3.89E-03	2.39E-03	4.34E-06
IBB-E 16	-156	Ca-Mg-HCO3-SO4	0.01	814	6.94	16.1	10.6	-3.1	1.00	1.13E-03	7.80E-05	2.70E-03	8.76E-04	4.34E-06
SGG 1	-	Na-Cl	0.66	59205	7.49	10.6	5.3	-0.3	1.03	6.27E-01	1.34E-03	6.28E-03	4.29E-03	4.96E-04
BE 1	-	Na-Cl	4.57	237610	5.72	14.9	2.4	0.5	1.16	4.33E+00	3.06E-03	5.63E-02	2.09E-02	5.04E-04
WK 1	-	Na-Cl	0.94	74384	5.79	18	2.8	-1.1	1.04	8.35E-01	3.87E-03	2.63E-02	6.45E-03	3.37E-04
WM 1	-	Na-Cl	0.94	74616	5.83	16	2.6	-0.3	1.04	8.32E-01	4.54E-03	3.08E-02	7.83E-03	4.75E-04
BBH 1	-	Na-Cl	4.43	230570	6.24	18.5	2.1	0.4	1.15	4.11E+00	1.67E-02	7.74E-02	2.48E-02	1.22E-03
BBH 2	-	Na-Cl	4.45	228330	6.25	25.6	2.2	0.5	1.15	4.14E+00	1.69E-02	7.70E-02	2.44E-02	1.28E-03
BBH 3	-	Ca-SO4-HCO3	0.05	2866	6.99	15	1.2	-3.3	1.00	2.19E-03	1.07E-04	1.42E-02	3.29E-03	1.36E-04
BBH 4	-	Ca-SO4-HCO3	0.05	2643	6.79	15	1.6	-3.2	1.00	1.92E-03	9.74E-05	1.31E-02	2.53E-03	1.96E-04
SGW 1	-	Ca-HCO3-SO4	0.01	700	7.71	16	4.6	-5.2	1.00	6.81E-04	7.31E-05	2.53E-03	6.02E-04	4.91E-06
SGW 2	-	Ca-HCO3	0.01	767	6.9	11.7	6.8	-11.4	1.00	5.24E-04	2.66E-05	2.75E-03	8.32E-04	2.74E-06
SGW 3	-	Ca-Mg-HCO3	0.01	755	6.02	11.8	4.2	-8.1	1.00	4.64E-04	7.20E-04	1.89E-03	1.09E-03	4.11E-06
SGW 4	-	Ca-K-NO3	0.004	320	4.74	11.6	6.0	1.7	1.00	4.06E-04	5.34E-04	5.80E-04	1.59E-04	5.71E-07
SGW 5	-	Ca-HCO3-Cl	0.008	603	6.76	11.9	4.1	-5.4	1.00	8.69E-04	3.76E-05	2.12E-03	2.05E-04	5.14E-06
SGW 6	-	Ca-HCO3-SO4	0.008	505	7.08	10.7	4.1	-5.3	1.00	4.82E-04	3.17E-05	1.97E-03	1.66E-04	4.68E-06

Sample ID	Ba	Li	Fe	Mn	Zn	Cu	Ni	B	Br	Cl	NO ₃ ⁻	SO ₄ ²⁻	HCO ₃ ⁻
	[mol/kg]	[mol/kg]	[mol/kg]										
IBB-W 1	1.89E-07	9.94E-05	3.04E-03	2.32E-04	8.41E-06	bdl	4.26E-06	6.48E-06	0.00E+00	4.52E-03	0.00E+00	1.67E-02	1.58E-03
IBB-E 1	7.67E-06	1.84E-03	2.33E-06	6.92E-06	2.60E-06	bdl	bdl	1.61E-04	9.17E-05	9.95E-01	4.50E-05	3.18E-03	1.40E-02
IBB-E 2	5.85E-06	1.98E-03	2.25E-04	1.46E-05	bdl	bdl	bdl	8.79E-05	1.31E-04	1.16E+00	9.21E-05	3.40E-03	6.01E-03
IBB-E 3	1.64E-06	3.14E-03	6.09E-04	4.82E-05	7.19E-06	bdl	bdl	2.51E-04	2.30E-04	3.10E+00	3.15E-05	2.24E-02	1.49E-03
IBB-E 4	3.60E-06	3.13E-03	1.23E-03	6.21E-04	9.48E-06	3.15E-06	bdl	7.59E-05	3.28E-04	2.45E+00	2.08E-05	1.42E-02	1.82E-03
IBB-E 5	3.86E-07	1.60E-04	5.37E-07	1.64E-06	bdl	bdl	bdl	2.68E-05	1.68E-05	1.38E-01	3.87E-05	6.58E-03	6.28E-03
IBB-E 6	8.37E-07	7.93E-04	4.12E-04	4.04E-05	7.65E-07	bdl	bdl	7.03E-05	7.88E-05	7.53E-01	bdl	1.45E-02	8.96E-03
IBB-E 7	7.86E-07	4.65E-04	2.52E-04	4.30E-05	1.53E-07	bdl	bdl	2.78E-05	4.77E-05	4.05E-01	1.79E-05	1.03E-02	6.60E-03
IBB-E 8	4.43E-06	7.31E-04	8.67E-05	3.40E-05	9.18E-07	bdl	bdl	3.15E-05	6.76E-05	5.81E-01	2.08E-05	7.10E-03	6.05E-03
IBB-E 9	6.28E-06	1.71E-03	3.15E-05	1.35E-05	1.22E-06	1.10E-06	bdl	5.00E-05	1.18E-04	1.03E+00	4.84E-05	4.28E-03	6.05E-03
IBB-E 10	2.11E-07	1.44E-05	3.58E-06	6.92E-06	1.53E-07	bdl	bdl	9.25E-06	bdl	6.47E-03	bdl	3.53E-03	4.56E-03
IBB-E 11	2.84E-07	1.87E-05	8.59E-06	1.97E-05	7.65E-07	1.57E-07	1.70E-07	3.70E-06	bdl	2.11E-03	5.74E-05	1.74E-03	2.86E-03
IBB-E 12	9.83E-07	0.00E+00	1.11E-04	3.19E-05	1.53E-07	bdl	bdl	bdl	bdl	3.68E-03	bdl	2.43E-03	2.52E-03
IBB-E 13	3.57E-07	2.02E-05	1.78E-04	2.57E-05	4.59E-07	bdl	1.70E-07	2.78E-06	bdl	1.80E-02	6.00E-05	1.31E-03	1.60E-03
IBB-E 14	1.67E-07	3.17E-05	7.28E-04	1.11E-04	bdl	bdl	1.53E-06	bdl	bdl	7.00E-03	bdl	7.79E-03	2.42E-03
IBB-E 15	2.33E-07	7.93E-05	3.77E-04	7.90E-05	5.81E-06	bdl	3.24E-06	5.55E-06	bdl	3.90E-03	bdl	6.31E-03	6.79E-04
IBB-E 16	1.46E-07	4.32E-06	1.43E-06	6.55E-06	4.59E-07	bdl	bdl	4.63E-06	bdl	1.62E-03	bdl	1.41E-03	4.44E-03
SGG 1	6.23E-05	7.40E-04	2.87E-06	7.28E-07	bdl	bdl	bdl	5.55E-04	2.41E-04	6.43E-01	3.10E-05	bdl	1.21E-02
BE 1	bdl	3.78E-03	6.07E-05	1.26E-05	bdl	bdl	bdl	3.15E-04	8.55E-04	4.41E+00	8.68E-05	1.85E-02	2.09E-03
WK 1	bdl	7.58E-04	1.63E-04	1.04E-05	bdl	bdl	bdl	2.51E-04	1.38E-04	8.38E-01	6.58E-05	2.46E-02	3.73E-02
WM 1	bdl	8.58E-04	3.25E-04	8.92E-06	bdl	bdl	bdl	2.75E-04	1.40E-04	8.34E-01	bdl	2.34E-02	3.95E-02
BBH 1	4.25E-06	4.51E-03	1.55E-04	2.97E-05	5.05E-06	bdl	bdl	3.42E-03	2.32E-03	4.28E+00	2.45E-04	7.64E-03	7.63E-04
BBH 2	3.98E-06	4.82E-03	1.53E-04	3.13E-05	3.06E-06	bdl	bdl	3.52E-03	2.30E-03	4.30E+00	1.79E-04	7.50E-03	6.69E-04
BBH 3	3.42E-07	9.80E-06	3.58E-07	3.46E-06	bdl	bdl	bdl	4.53E-05	1.50E-06	1.67E-03	4.03E-06	1.50E-02	7.87E-03
BBH 4	2.48E-07	7.06E-06	1.25E-06	3.82E-06	bdl	bdl	bdl	3.52E-05	1.63E-06	2.17E-03	6.29E-06	1.26E-02	8.14E-03
SGW 1	1.31E-06	2.59E-06	4.66E-06	3.09E-06	3.37E-07	bdl	bdl	2.78E-06	1.25E-06	1.06E-03	1.12E-04	1.33E-03	3.93E-03
SGW 2	4.59E-07	1.01E-06	bdl	bdl	1.07E-07	bdl	bdl	9.25E-07	5.01E-07	4.54E-04	3.59E-04	1.46E-04	8.54E-03
SGW 3	5.97E-07	8.65E-07	4.08E-05	2.04E-04	9.18E-08	bdl	bdl	2.78E-06	1.13E-06	7.04E-04	6.94E-06	6.88E-04	6.85E-03
SGW 4	6.33E-07	4.32E-07	1.79E-07	1.13E-05	7.65E-07	bdl	bdl	2.78E-06	7.51E-07	5.09E-04	1.48E-03	2.53E-04	2.62E-05
SGW 5	3.28E-07	1.15E-06	8.25E-05	1.00E-05	bdl	bdl	bdl	9.25E-07	6.26E-07	1.86E-03	2.74E-06	2.46E-04	4.05E-03
SGW 6	4.30E-07	1.29E-04	2.3E-05	6.4E-06	bdl	bdl	bdl	1.9E-06	5.0E-07	7.2E-04	1.3E-06	9.1E-04	2.81E-03

Sample ID	SI _{Calcite}	P _{CO2} (atm)	SI _{Gypsum}	SI _{Halite}	δD [‰]	δ ¹⁸ O (H ₂ O) [‰]	δ ¹⁸ O (SO ₄) [‰]	SD [‰]	δ ³⁴ S [‰]	SD [‰]	⁸⁷ Sr/ ⁸⁶ Sr	³ H TU	SD TU	Na/Cl	Cl/Br
IBB-W 1	-1.3	10 ^{-1.5}	-0.3	-6.1	-51.3	-7.73	0.20	0.4	-4.00	0.1	0.71102	5.9	1.0	2.162	-
IBB-E 1	0.4	10 ^{-1.3}	-1.7	-2.0	-53.0	-7.98	11.20	0.3	18.00	0.0	0.71188	0.9	0.8	0.975	10846
IBB-E 2	-0.3	10 ^{-1.2}	-1.7	-1.8	-51.1	-7.72	9.60	0.1	17.10	0.2	0.71275	<i>n.m.</i>		0.974	8892
IBB-E 3	-0.9	10 ^{-1.3}	-0.7	-0.9	-58.6	-8.65	11.50	0.0	21.10	0.1	0.71078	<0.6	-	0.974	13457
IBB-E 4	-0.3	10 ^{-1.9}	-0.7	-1.1	-48.3	-7.14	10.80	0.7	20.10	0.1	0.71346	<0.6	-	0.945	7465
IBB-E 5	0.3	10 ^{-2.0}	-0.9	-3.5	-53.1	-8.02	4.50	0.1	5.80	0.3	0.71088	3	0.9	0.973	8244
IBB-E 6	0.2	10 ^{-1.2}	-0.5	-2.2	-56.2	-8.30	10.10	0.3	17.50	0.3	0.71050	1.3	0.7	0.920	9553
IBB-E 7	-0.1	10 ^{-1.3}	-0.6	-2.7	-53.3	-8.03	7.20	0.4	9.30	0.1	0.71074	3.5	0.8	0.917	8499
IBB-E 8	0.1	10 ^{-1.7}	-1.0	-2.4	-52.2	-7.88	7.90	0.1	12.60	0.3	0.71183	1.7	0.8	0.951	8601
IBB-E 9	0.2	10 ^{-1.8}	-1.5	-1.9	-48.5	-7.32	8.30	0.3	18.80	0.2	0.71279	1.6	0.8	0.959	8766
IBB-E 10	0.6	10 ^{-2.5}	-1.0	-6.0	-51.5	-7.93	2.50	0.8	-3.80	0.0	0.71034	2.4	1.1	1.079	-
IBB-E 11	-0.4	10 ^{-2.0}	-1.3	-7.1	-46.0	-6.90	0.20	0.1	-1.90	0.1	0.70910	4	0.9	0.725	-
IBB-E 12	-1.0	10 ^{-1.6}	-1.2	-6.6	-50.8	-7.70	-2.20	0.2	0.30	0.5	0.71036	5.3	0.8	0.819	-
IBB-E 13	-0.9	10 ^{-2.1}	-1.5	-5.3	-50.8	-7.69	0.00	0.1	-1.00	0.0	0.71081	5.2	1.0	0.758	-
IBB-E 14	-0.9	10 ^{-1.5}	-0.5	-6.1	-53.5	-8.15	-2.40	0.1	-3.80	0.6	0.71062	<i>n.m.</i>		0.745	-
IBB-E 15	-1.7	10 ^{-1.9}	-0.7	-6.5	-50.6	-7.70	-1.20	0.7	-4.40	0.2	0.71052	<i>n.m.</i>		0.883	-
IBB-E 16	-0.3	10 ^{-1.6}	-1.4	-7.4	-52.2	-7.96	-0.90	0.6	-8.30	0.0	0.71035	<i>n.m.</i>		0.700	-
SGG 1	0.4	10 ^{-1.9}	-	-2.3	-42.39	-6.64	<i>bdl</i>	<i>bdl</i>	<i>bdl</i>	1.0	0.70909	<i>n.m.</i>		0.975	2672
BE 1	-0.6	10 ^{-1.0}	-0.2	-0.5	-50.15	-8.28	14.3	0.2	21.4	0.3	0.70819	<i>n.m.</i>		0.982	5153
WK 1	-0.1	10 ^{0.3}	-0.3	-2.1	-57.47	-8.92	11.6	0.1	13	0.2	0.70994	<i>n.m.</i>		0.996	6058
WM 1	0.0	10 ^{0.3}	-0.3	-2.1	-61.92	-9.13	11.3	0.6	12.8	0.2	0.70965	<i>n.m.</i>		0.998	5938
BBH 1	-0.4	10 ^{-2.0}	-0.5	-0.5	-14.59	-2.73	12.8	0.3	28.3	0.0	0.71038	<i>n.m.</i>		0.959	1842
BBH 2	-0.4	10 ^{-2.1}	-0.5	-0.5	-14.32	-2.69	11	0.7	27.5	0.2	0.71039	<i>n.m.</i>		0.962	1870
BBH 3	0.5	10 ^{-1.4}	-0.1	-7.2	-43.69	-6.66	17.7	0.7	19.9	0.6	0.70830	<i>n.m.</i>		1.306	1115
BBH 4	0.3	10 ^{-1.2}	-0.1	-7.1	-45.12	-6.94	16.1	0.2	19.1	0.2	0.70832	<i>n.m.</i>		0.884	1334
SGW 1	0.4	10 ^{-2.4}	-1.4	-7.8	-50.58	-7.85	5.1	0.6	-15.3	0.1	0.70930	<i>n.m.</i>		0.640	850
SGW 2	0.0	10 ^{-1.3}	-2.3	-8.3	-48.31	-6.83	10.4	0.3	4.7	0.5	0.70874	<i>n.m.</i>		1.154	907
SGW 3	-1.2	10 ^{-0.5}	-1.8	-8.1	-47.33	-6.87	14.2	0.4	5.4	0.0	0.71191	<i>n.m.</i>		0.659	625
SGW 4	-5.1	10 ^{-1.4}	-2.5	-8.3	-46.50	-6.41	8.6	0.2	19.3	0.8	<i>n.m.</i>	<i>n.m.</i>		0.797	678
SGW 5	-0.6	10 ^{-1.5}	-2.1	-7.4	-48.80	-6.61	15.3	0.1	31	0.4	0.70862	<i>n.m.</i>		0.467	2971
SGW 6	-0.5	10 ^{-1.9}	-1.6	-8.1	-49.20	-6.52	8.6	0.7	18.6	0.0	0.70839	<i>n.m.</i>		0.666	1446

Table S1: Physical and chemical parameters of water samples. I = Ionic strength; EC₂₅ = calculated electrical conductivity at 25 °C using the phreeqc.dat database; Temp = temperature; DO = dissolved oxygen; CBE = charge balance error; bdl = below detection limit; n.m. = not measured; SD = standard deviation; SI = Saturation index; TU =Tritium units. Density was calculated using the computercode PHREEQC together with the phreeqc.dat database.